Journal of Solar Energy Research (JSER)

Journal homepage: www.jser.ut.ac.ir

Comparative Study and Optimization of a Solar Combined Power and Natural Gas Liquefaction Cycle Equipped with Various Ejector Refrigeration Loops

Arezoo Sohbatloo[a], Fateme Ahmadi Boyaghchi[a,*]

[a]Department of Mechanical Engineering, Faculty of Engineering and Technology, Alzahra University, Tehran, Iran
*E-mail: fahmadi@alzahra.ac.ir

ARTICLE INFO

Received in revised from: *2019/6/30*

Accepted: *2019/7/26*

Keywords:
Perturbation, solar irradiance, semiconductor temperature, photovoltaic parameters, output current and voltage, thermal conductance and resistance.

A B S T R A C T

This research develops and analyses three combinations of a solar driven cascade organic Rankine cycle (CORC) with ejector refrigeration loop (ERL) to produce power and liquefied natural gas (LNG) using exergy, exergoeconomic and exergoenvironmental concepts. In Case I, the extracted streams from turbines are used as ejectors primary fluids, in Case II, the ejector in high temperature (HT) loop is inserted after turbine and in Case III both ejectors are installed before the turbines. A comparative study is conducted to evaluate the performances of the proposed layouts. The simulation results demonstrate that Case III gives the lowest total product cost rate of 78.372 $/h and Case II causes the maximum energy and exergy efficiencies of 14.3% and 7.101%, respectively. Moreover, in this layout, the cost and environmental impact (EI) per exergy unit of LNG are improved by about 0.003 $/GJ and 17 mPts/GJ, respectively in relation to Case I. Finally, the ultimate solution of Case II as the best layout is ascertained and compared with Case I by applying Non-dominated Sorting Genetic Algorithm II (NSGA-II) and three decision makers, namely LINMAP, TOPSIS and Shannon Entropy. According to the optimization results, the maximum improvements in product cost rates are achieved within 1.2% and 2.2% for cases I and II, respectively and the maximum reduction in EI rate for Case I is obtained within 1.05% through LINMAP method.

1. Introduction

ORC is a technology converting low-grade heat sources such as industrial waste heat, solar energy, biomass and geothermal energy into high-grade power energy by applying a low-boiling temperature organic material as the working fluid [1]. To enhance the performance of the traditional ORC, a new ORC configuration called cascade ORC (CORC) was developed in which the coolant waste heat in HT ORC loop was utilized to drive low temperature (LT) ORC loop in order to produce additional power [2-6]. To achieve a better thermodynamic performance of CORC, a regenerator was applied in the HT ORC loop [7].

In recent years, many researches have been devoted to study ORC-based combined cycles in order to satisfy both cooling and power needs. Regarding to the traditional ORC combined cooling and power (CCP) cycle, cooling effect can be produced using an absorption refrigeration cycle [8-11] or ejector refrigeration loop (ERL). An ERL is a promising way of producing cooling effect because an ejector with simple and no moving parts has several advantages such as: improving the coefficient of performance, low operational and maintenance costs and ability to operate with various refrigerants [12-16].

Several studies on ORC CCP with special place for insulation of the ejector have been reported in the literature. For instance, Wang et al. [17] proposed and analyzed thermodynamically an ORC CCP with R123 as working fluid. In this design, the extracted vapor from the turbine acted as the primary fluid of the ejector and the room space got cooled by cooling effect produced in evaporator. Similar configuration for the ejector location was constructed by Habibzadeh et al. [18]. In this research, the effects of various organic working fluids were evaluated on the performance of the system. Zheng and Weng [19] designed an ORC CCP at which the expanded fluid exiting turbine entered the ejector as primary fluid and water got cooled in the evaporator. The thermodynamic performances of the proposed system were studied by applying different organic fluids.

Ahmadzadeh et al. [20] investigated an ORC CCP integrated with evacuated tube solar collectors. Partially expanded working fluid exiting the turbine was applied as the ejector primary fluid. Thermodynamic performance of the proposed system was evaluated and a thermo-economic analysis was conducted using the SPECO (specific exergy costing) method. Rostamzadeh et al. [21] proposed and compared the performances of four appropriate combination of ORCs with a distinct ERL at which the energy of ejector primary fluid was provided from the stream leaving turbine via a heat exchanger. Rostamzadeh et al. [22] designed two ORC CCPs in which ERL was used to produce cooling load at three and two[23] temperature levels for freezing, refrigeration and air-conditioning usages and power was produced using an ORC and recuperative ORC with turbine bleeding. In all layouts, ERL was cascaded with the condenser of ORC. The proposed cycles were analyzed and optimized by applying thermodynamic and exergoeconomic concepts. All configurations provided the space cooling for domestic applications.

For industrial application, a combination of CORC instead of traditional ORC with ERLs was proposed to liquefy the NG. In this research, solar energy was employed using linear Fresnel collector (LFC) and two ERLs were installed in HT and LT ORC loops. The primary fluids of EJCs were provided by streams extracted from turbines [24].

To the best of our knowledge and surveying the mentioned literature review, the combination of ORC or CORC CCP with various ERLs has not been performed so far. The novelty of this work is to design new locations for ERLs by combining all possible cases for driving ERLs, i.e. using stream before turbines, extracted stream of turbines or stream exiting turbines, in an existing solar driven CORC CCP based LNG cycle [24] (Case I) for an industrial application. The main objectives of this study are pinpointed as follows:

a) To conduct the energy, exergy, exergoeconomic and exergoenvironmental concepts for all cases.
b) To determine and compare the thermodynamic, economic and EI performances of the desired cases during a year.
c) To identify the superiority of each case from the energy, exergy, exergoeconomic and exergoenvironmental perspectives.
d) To select the best layout by considering the aforementioned perspectives.To assess and compare the performances of the selected case in comparison with Case I by conducting a parametric study.

e)To optimize and compare the performances of the selected cases by applying LINMAP, TOPSIS and Shannon entropy decision makers from the Pareto frontier obtained by NSGA-II.

2. Cycle description

Figure 1 illustrates the schematic diagram of a solar power/LNG production system with various ERL configurations and with various cases and their T-s diagrams. The desired systems consist of an LFC field as more cost effective concentrating collector [25-30], three TSTs, a CORC, two ERLs placed in LT and HT cycles and NG process line. In the basic configuration denoted as Case I, the primary flow of the ejectors are provided from the streams extracted from TURs [24] while in Case II, EJC-1 is installed at the exit of TUR-1 and in Case III, both ejector are placed before TURs and the primary flow is the fraction of TURs entrance flows. In this study, R227ea and R32 with zero ozone depletion potential (ODP) and non-toxin organic fluids are selected for HT and LT loops [31], respectively.

The detailed operations of the systems are described as follows: The R227ea saturated liquid in HT ORC cycle is pressurized through P-1 (states 1 and 2) and then enters PRC-1 to cool the high pressure NG (states G1 and G2). The warm working fluid passes through HHE-2 and HHE-1 where it gets super-heated (states 3-5) by absorbing the thermal energy of hot Therminol-PV1 flowing inside the solar subsystem (states E1-E3). The high pressure and superheated R227ea flows into TUR-1 to produce power. The two-phase flow thermal energy leaving TUR-1 (state 7) is used to preheat the working fluid inside the LT ORC loop via CHE and R227ea gets liquid saturated via CON-1 by rejecting heat to NG (states G9 and G10). Then stream reenters P-1 to complete the HT ORC loop. In LT ORC loop, the pressure of R32 saturated liquid increases by P-2 (states 15 and 16) and it is preheated by cooling NG via PRC-2 and by absorbing the heat of two-phase flow exiting TURs via REG and CHE and then it is superheated by receiving thermal energy from Therminol-PV1 (states E3 and E4) inside LHE-1 (states 15-20). The superheated R32 produces power when passing through TUR-2 and gets liquid saturated (states 22-24) by losing heat inside REG and CON-2 by rejecting heat to LNG (states G8 and G9). On the other hand, to liquefy the precooled NG, each ORC cycle is equipped by ERL. In Case I, a part of stream passing through TURs is extracted and enters the drive nozzle of EJCs as primary fluid (states 14 and 29). The primary stream jetting from ejector nozzle (state a) sucks the low temperature and pressure vapor fluid leaving EVAs (states 12 and 27) with a pressure reduction (state b). The two stream are mixed in the ejector at constant pressure (state c) as shown in Figure 2. Then, the mixed flow leaves the ejector diffuser with a pressure rise (states 13 and 28). The precooled NG is discharged into EVA-1, PRC-2 and EVA-2 and gets liquid completely (states G2- G6). A portion of LNG is extracted to produce cooling medium for CONs (states G8-G10) and then returned to EVP-2. In Case II, EJC-1 is placed after TUR-1. In this way, the leaving two-phase fluid is sent to EJC-1 as primary fluid and in Case II both EJCs are installed before TURs and a portion of stream entering TURs flows into EJCs as primary fluid.

2. Energy methods

Energy analysis is performed by considering several assumptions:

- All components operate under the steady state condition.
- The kinetic energy is negligible for all components except ejectors.
- The potential energy is neglected for all components.
- The pressure drops inside pipelines and all components except LFC are negligible.
- No heat transfer with environment occurs for the pipelines and all components except LFC and TST.
- The process through the TV is isenthalpic.
- The environmental temperature and pressure are taken to be 298.15 K and 101.325 kPa, respectively.
- The isentropic efficiencies for TURs and Ps are taken to be 0.85 and 0.95, respectively.
- P-1 and P-2 entrance streams are considered as saturated liquid and EVAs outlet streams are saturated vapor.

For steady flow components, the mass rate balance can be written as:

$$\sum \dot{m}_{in} = \sum \dot{m}_{out} \tag{1}$$

and the energy rate balance can be written as:

$$\dot{Q}_{in} + \dot{W}_{in} + \sum \dot{m}_{in} h_{in} = \dot{Q}_{out} + \dot{W}_{out} + \sum \dot{m}_{out} h_{out} \tag{2}$$

In Eqs. (1) and (2), $\dot{m}$ is mass flow rate, $\dot{Q}$ is heat transfer rate, $\dot{W}$ is power and h is enthalpy. The indexes "*in*" and "*out*" indicate the input and output streams.

The energy rate balance for LFC, EJCs and TST can be written in different ways as follows:

1.1. Ejector simulation

The ejectors can be classified into constant-pressure and constant-area types. According to the studies reported in the literature, the performance of the constant-pressure mixing ejector is better than that of the constant-area one [12, 32, 33]. Figure 2 indicates the constant-pressure mixing ejector containing the motive nozzle, suction chamber, constant area section and diffuser section. By neglecting the velocities of inlet and outlet streams of the ejector and considering the friction losses inside nozzle, mixing and diffuser sections in terms of efficiencies, the mathematical model is established for the one-dimensional constant-pressure ejector by Eqs. (3) to (16):

1.1.1. At the motive nozzle outlet

$$h_{a,is} = h\left(P_a, s_1\right) \tag{3}$$

$$h_a = h_1 - \eta_{mn}\left(h_1 - h_{a,is}\right) \tag{4}$$

Here, η_{mn} is the isentropic efficiency of the motive nozzle, set to be 0.85.

$$V_a = \sqrt{2\left(h_1 - h_a\right)} \tag{5}$$

where V indicates the stream velocity.

$$A_{1b} = \frac{1}{\left(1+\mu\right)\rho_a V_a} \tag{6}$$

In Eq. (6), μ is the entrainment ratio defined as the ejector suction mass flow rate to motive mass flow and ρ refers to the fluid density.

1.1.1. At the suction nozzle outlet

$$h_{b,is} = h\left(P_b, s_2\right) \tag{7}$$

$$h_b = h_2 - \eta_{sn}\left(h_2 - h_{b,is}\right) \tag{8}$$

Here, η_{sn} is the isentropic efficiency of the suction nozzle, given to be 0.85.

$$A_b = \frac{1}{\left(1+\mu\right)\rho_b V_b} \tag{9}$$

1.1.2. In the mixing section

$$V_c = \sqrt{\eta_{ms}}\left(\frac{1}{1+\mu}V_a + \frac{\mu}{1+\mu}V_b\right) \tag{10}$$

Here, η_{ms} is the isentropic efficiency of the mixing section, given to be 0.95.

$$h_c = \frac{1}{1+\mu}\left(h_a + \frac{V_a^2}{2}\right) + \frac{\mu}{1+\mu}\left(h_b + \frac{V_b^2}{2}\right) - \frac{V_c^2}{2} \tag{11}$$

$$s_c = s\left(P_c, h_c\right) \tag{12}$$

1.1.3. At the diffuser outlet

$$h_3 = h_c + \frac{V_c^2}{2} \tag{13}$$

$$h_{3,is} = h_c - \eta_d\left(h_3 - h_c\right) \tag{14}$$

where η_d is the isentropic efficiency of the diffuser outlet with value of 0.85.

$$P_3 = P\left(h_{c,is}, s_c\right) \tag{15}$$

The entrainment ratio of the ejector can be calculated by iteration with known values of P_1, P_2, ΔP and efficiencies until the quality of fluid (x) at the exit of ejector is valid.

$$x_3 = \frac{1}{1+\mu} \tag{16}$$

1.2. LFC simulation

An LFC mainly contains long, thin and flat segments of mirror as the first flat reflectors, a fixed tubular receiver enveloped by the vacuumed glass cover and a parabolic cavity as the second reflector. The mirrors sloped with tilt

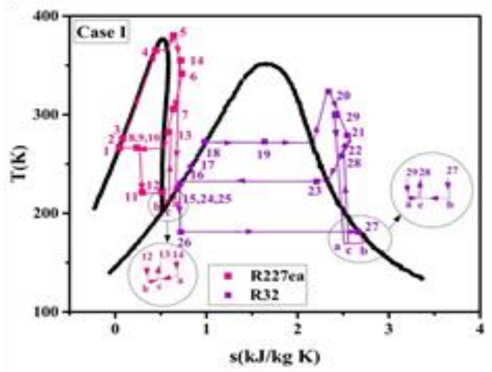

a) Case I

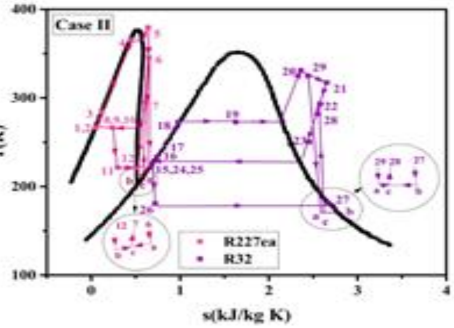

Case II

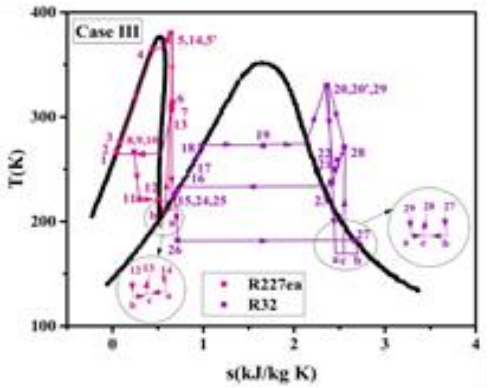

b) Case III

Figure 1. Schematic assembly of solar driven NG liquefaction plant with various configurations of ERL[24] and their T-s diagrams a) Case I, b) Case II and c) Case III

angle of θ can track the position of the sun in the sky from East to West to concentrate the solar energy onto the fixed receiver located at the focal point of the reflectors [34].

The useful heat energy gain $\dot{Q}_u$ by Therminol-PV1 can be determined using Eqs. (17) to (19) [34]:

$$\dot{Q}_u = \dot{m}_{oil} C_P \left(T_{out} - T_{in}\right) = A_{ap}\left[S - \frac{U_L}{C}\left(T_r - T_{air}\right)\right] \tag{17}$$

Here, $\dot{m}$ is mass flow rate, C_P is specific heat, T is temperature, A_{ap} represents the aperture area, the subscript oil indicates Therminol-PV1. U_L refers to the overall heat loss coefficient from the receiver to the environment which can be calculated using the correlations expressed in [34]. In Eq. (17), the subscripts, *r* and *air* are the receiver and air, respectively. *S* and *C* indicate the absorbed solar heat and the concentration ratio expressed by Eqs. (18) and (19), respectively.

$$S = G_b \gamma_1 \gamma_2 \tau_g \alpha_r r \tag{18}$$

Where G_b is beam radiation falling on a horizontal surface, γ_1 is the reflectivity of the first flat reflector, γ_2 is the reflectivity of the second parabolic reflector (given to be 0.93), τ_g refers to the transitivity of the glass envelope (set to be 0.95), α is the absorptivity of the receiver (set to be 0.95) and r is shading factor.

$$C = \frac{A_{ap}}{A_r} = 2 \times \sum_{n=1}^{n=m} \frac{w\cos\theta_n}{\pi D_i} \tag{19}$$

In Eq. (19), A_r is the receiver area. *w* refers to the width of the constituent mirror elements, θ_n is the tilt angle of mirrors, D_i is the inner diameter of receiver and *n* indicates the mirror number.

A TST is mounted in solar subsystem to operate as a buffer between LFC field and CORC subsystem. The temperature of Therminol-PV1 at the exit of TST can be calculated by assuming the well-mixed model and correlations expressed by Wang et al. [35].

3. Exergy-based methods

An exergy analysis is a convenient tool to identify the location, magnitude and causes of thermodynamic rreversibilities within the *k*th component of energy conversion system and the exergy loss due to the exergy transfer to the environment. The exergy associated with each stream of the overall system can be calculated using the exergy balance with concepts of fuel and product for the *k*th component as follows [36]:

$$\dot{E}x_{F,k} = \dot{E}x_{P,k} + \dot{E}x_{D,k} + \dot{E}x_{L,k} \tag{20}$$

Here, $\dot{E}x\left(=\dot{m}\,ex\right)$ indicates the physical and chemical exergy streams divided into the thermal component (ex^T) and mechanical component (ex^M) for stream that its temperature is lower than dead state [36]. The indexes *F*, *P*, *D* and *L* denote the fuel, product, destruction and losses, respectively.

The exergy destruction ratio of the each component, $y_{D,k}$, can be calculated using Eq. (21):

$$y_{D,k} = \frac{\dot{E}x_{D,k}}{\dot{E}x_F^{tot}} \tag{21}$$

Exergoeconomic analysis is the combination of exergy and cost concepts providing the designer or operator of a system with information crucial to the design or operation of a cost effective system [36, 37]. A cost balance applied to the *k*th system components shows that the sum of cost

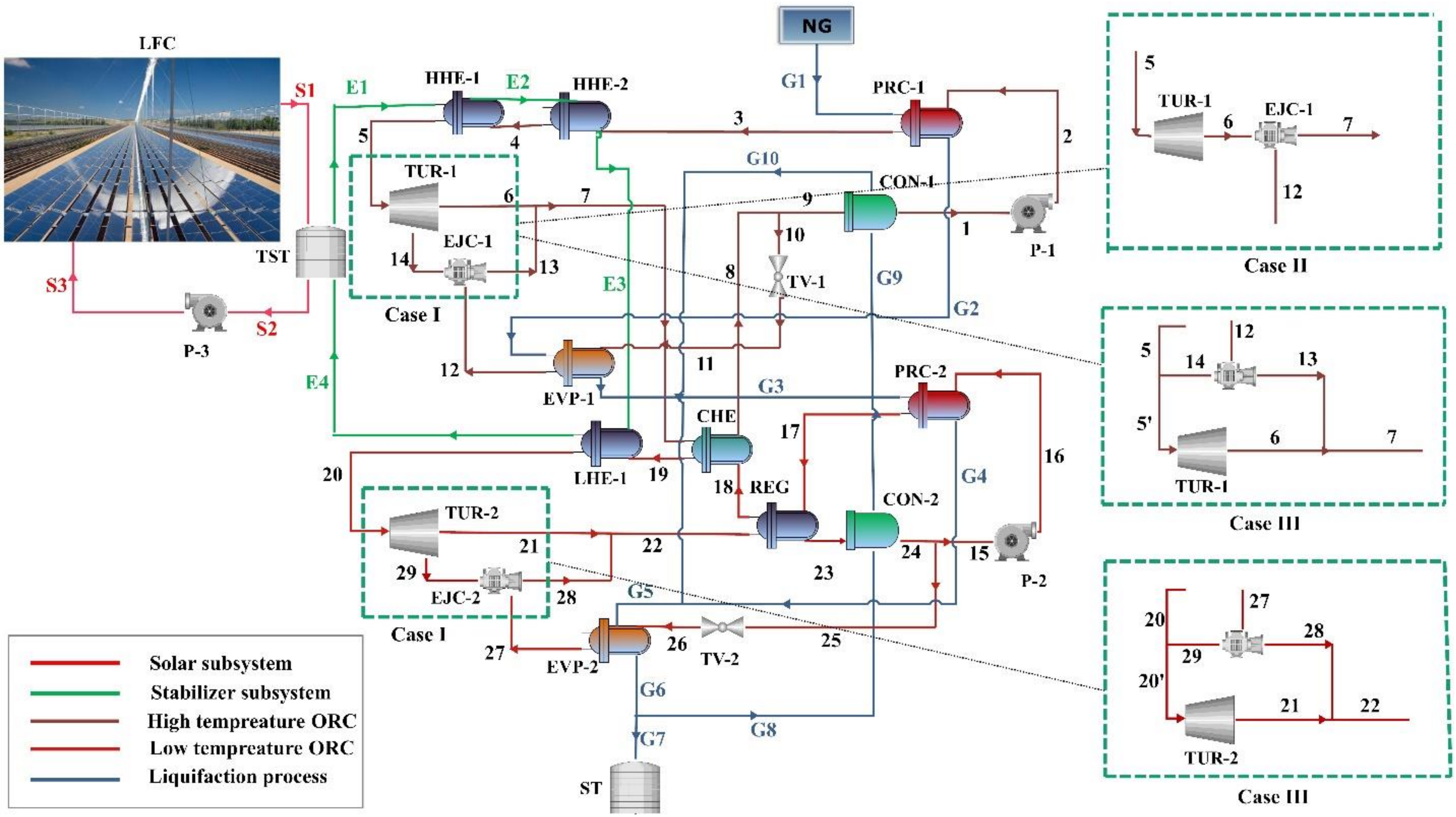

LFC
NG
G1
PRC-1
HHE-1
E2
HHE-2
E1
S1
S2
S3
TST
P-3
TUR-1
EJC-1
Case I
Case II
Case III
CON-1
TV-1
P-1
G10
G9
G2
G3
E3
E4
EVP-1
CHE
PRC-2
LHE-1
REG
CON-2
P-2
G4
TUR-2
EJC-2
G5
EVP-2
TV-2
G6
G7
G8
ST
TUR-2
Solar subsystem
Stabilizer subsystem
High tempreature ORC
Low tempreature ORC
Liquifaction process

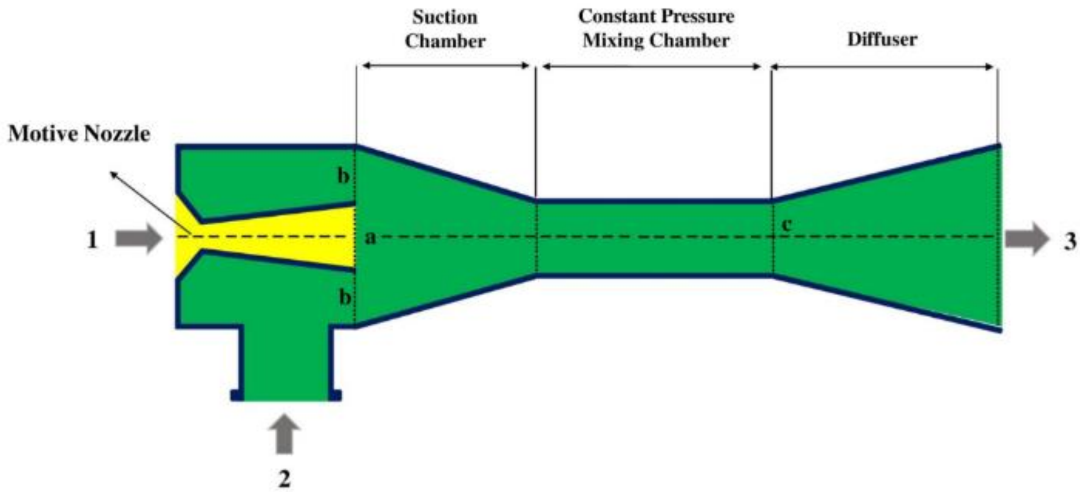

rates associated with all existing exergy stream equals the sum of cost rates of all entering exergy streams plus the appropriate charges due to capital investment and operating and maintenance expenses[38]. The cost balance of the *k*th component can be written based on the specific exergy costing approach as follows:

$$\sum_{out}\dot{C}_{out,k}+\dot{C}_w=\dot{C}_{q,k}+\sum_{in}\dot{C}_{in,k}+\dot{Z}_k \tag{22}$$

$$\dot{C}_{in}=c_{in}\dot{E}x_{in} \tag{23}$$

$$\dot{C}_{out}=c_{out}\dot{E}x_{out} \tag{24}$$

$$\dot{C}_w=c_w\dot{W} \tag{25}$$

$$\dot{C}_q=c_q\dot{E}x_q \tag{26}$$

where c is the average cost per unit of exergy. $\dot{C}$ denotes the cost stream associated with the corresponding exergy stream. The indexes *in* and *out* refer to the entering and exiting streams of matter. The indexes *w* and *q* refer to the power and heat transfer rates.

The $\dot{Z}$ appeared in Eq. (22) is the cost rate associated with the capital investment and operating and maintenance expenses, which can be written as:

$$\dot{Z}_k=\frac{Z_k\times\varphi\times CRF}{N} \tag{27}$$

Here, φ is the maintenance factor and *CRF* refers to the capital recovery factor being expressed by [36]:

$$CRF=\frac{IR\left(1+IR\right)^N}{\left(1+IR\right)^N-1} \tag{28}$$

$$f_{c,k}=\frac{\dot{Z}_k}{\dot{Z}_k+\dot{C}_{D,k}} \tag{31}$$

In Eq. (28), *IR* and *N* are respectively the interest rate and the system life. Table 1 indicates the values of economic parameters and the purchased equipment costs of components are presented in Appendix A.

In exergoeconomic analysis, it is assumed that the average cost per unit of entering exergy streams are known for all entering streams. Consequently, the unknown variables to be calculated from a cost balance for the *k*th component are the costs per exergy unit of the exiting material streams. Therefore, n-1 auxiliary relations are required for components with n exiting exergy streams. These relations

can be written using Fuel and Product rules detailed in[36]. Table 2 indicates the cost balance with corresponding auxiliary equations of each component. By solving the cost balances and auxiliary equations, simultaneously, all average cost per unit of exergy streams of a system can be calculated.

The evaluation of each component from the exergoeconomic viewpoint can be carried out by applying Eqs. (29), (31) and (32).

$$\dot{C}_{D,k}=c_{F,k}\dot{E}x_{D,k} \tag{29}$$

In Eq. (29), $\dot{C}_D$ indicates the cost associated with the exergy destruction in a component or process and c_F is the cost per exergy of fuel which can be calculated by:

$$c_{F,k}=\frac{\dot{C}_{F,k}}{\dot{E}x_{F,k}} \tag{30}$$

Here, $\dot{C}_{F,k}$ is the cost rate associated with the fuel which is obtained by replacing the exergy ($\dot{E}x$) by cost rate $\dot{C}$ in the fuel exergy of the each component.

$$\dot{B}_{D,k}=b_{F,k}\dot{E}x_{D,k} \tag{35}$$

Here, $f_{c,k}$ is the exergoeconomic factor indicating the contribution of the component-related investment cost rate, $\dot{Z}_k$, to the total cost of the component, $\dot{Z}_k + \dot{C}_{D,k}$ A low value of the exergoeconomic factor calculated for a major component suggests that cost saving in the entire system might be achieved by improving the component efficiency. A high value of this factor suggests a decrease in the investment costs of this component at the expense of its exergetic efficiency [36].

$$r_{c,k} = \frac{c_{P,k} - c_{F,k}}{c_{F,k}} \tag{32}$$

where, $r_{c,k}$ is the relative cost difference. This variable express the relative increase in the average cost per exergy unit between fuel and product of the component ($c_{P,k}$). The relative cost difference represents the cost reduction potential within the kth component. The value of $c_{P,k}$ can be estimated by following relation:

$$c_{P,k} = \frac{\dot{C}_{P,k}}{\dot{E}x_{P,k}} \tag{33}$$

In Eq. (33), $\dot{C}_{P,k}$ is the cost rate associated with the product which is obtained by replacing the exergy ($\dot{E}x$) by cost rate $\dot{C}$ in the product exergy of the each component.

Table 1. Economic parameters [39].

Parameter	Value
φ	1.06
IR	10%
N	20 year

An exergoenvironmental analysis combines the exergy analysis and life cycle assessment (LCA) to identify the EI of exergy streams. The EI balances for the kth component can be written as [40]:

$$\sum_{in} \dot{B}_{in,k} + \dot{Y}_k = \sum_{out} \dot{B}_{out,k} \tag{34}$$

Here, $\dot{B}\left(= b\dot{E}x\right)$ is the EI rate associated with the exergy stream, b is the average EI per unit of exergy.

The $\dot{Y}_k$ appeared in Eq. (34), indicates the component-related EI of the kth component comprising the construction, operation and maintenance and the disposal of the component identified by LCA based on based on Eco-indicator 99. Table 2 indicates the EI balance with corresponding auxiliary equations of each component.

To assess the system components EI, three criteria are defined as follows:

where, $\dot{B}_D$ is the EI of exergy destruction rate within the kth component and b_F indicates the EI per exergy of fuel.

$$f_{b,k} = \frac{\dot{Y}_k}{\dot{Y}_k + \dot{B}_{D,k}} \tag{36}$$

Here, $f_{b,k}$ is the exergoenvironmental factor within the kth component expressing the contribution of the component-related EI, $\dot{Y}_k$, to the total EI of the component, $\dot{Y}_k + \dot{B}_{D,k}$.

$$r_{b,k} = \frac{b_{P,k} - b_{F,k}}{b_{F,k}} \tag{37}$$

In Eq. (37), $r_{b,k}$ is the relative EI difference, indicating the EI reduction potential within the kth component and b_P is the EI per exergy of product.

4. Performances

The average annual energy efficiency of the system is defined as:

$$\eta_{En} = \frac{\dot{W}_{net} + \dot{Q}_{LNG}}{A_{ap} G_b} \tag{38}$$

The average annual power efficiency of the system is defined as:

$$\eta_{En} = \frac{\dot{W}_{net}}{A_{ap} G_b} \tag{39}$$

The average annual exergy efficiency of the system can be calculated by:

$$\eta_{Ex} = \frac{\dot{W}_{net} + \dot{m}_{LNG}\left[ex_{G-7}^{T} - ex_{G-1}^{T}\right]}{\dot{E}x_{F,LFC} + \dot{m}_{LNG}\left[ex_{G-1}^{M} - ex_{G-7}^{M}\right]} \tag{40}$$

The total product cost rate associated with power and LNG production can be calculated by:

$$\dot{C}_P^{tot} = \dot{C}_{P,LNG} + \dot{C}_{P,TUR-1} + \dot{C}_{P,TUR-2} \tag{41}$$

The EI rates of system can be written as:

$$\dot{B}_P^{tot} = \dot{B}_{P,LNG} + \dot{B}_{P,TUR-1} + \dot{B}_{P,TUR-2} \tag{42}$$

5. Multi-objective Optimization procedure

In this investigation, NSGA-II evolutionary algorithm proposed by Deb [41] is employed to find the optimum annual performances and design parameters of the proposed systems.

The flow chart of NSGA-II algorithm is illustrated in Figure 3.

The energy efficiency and exergy efficiency, cost and EI rates of the systems which are assessed by Eqs. (38) to (40) are considered as four objective functions. In this regard, ten and nine major design parameters respectively for Case I and Case II listed in Table 3 with corresponding boundaries are selected as decision variables. Meanwhile, tuning parameters of genetic algorithm used for convergence of the results are listed in Table 4.

To find the optimum solution from the Pareto frontier, the most recognized decision makings including Shannon Entropy, LINMAP and TOPSIS procedures are employed in parallel.

Detail descriptions of the Shannon Entropy, LINMAP and TOPSIS decision makers can be found in Refs. [42-45].

2. Results and discussion

According to the assumptions made in section 2 and input parameters listed in Table 5, simulations of the proposed systems are performed by developing codes in Engineering Equation Solver (EES) software to solve the governing equations and R227ea and R32 properties. A parametric study is also carried out to determine the positive effects of varying several important parameters on the thermodynamic, economic and environmental performances of all cases.

The results of various ERLs on the performances of the system are tabulated accordingly in Table 6. The outcomes show that mounting the ejector at the exit of TUR-1, i.e. Case II, improves the produced cooling load of liquefaction within 1.9 times in relation to Case I due to increase of LNG capacity.

Moreover, the produced LNG exergy gets 1.82 times while these values are lower in other cases. In this manner, the mass flow rate of produced LNG gets within 4 kg/s and energy and exergy efficiencies increase by about 43.3% and 9.5%, respectively.

Obviously, Case I gives the maximum power efficiency of 4.11% followed by cases III and II, respectively. The amount of total product cost rate of Case III is lower than that of other cases. Indeed, when the primary streams for EJCs are provided from the streams before TURs, the cost per exergy of TURs drops. The highest value of $\dot{B}_P^{tot}$ belongs to Case II because the LNG exergy rate is higher than that of other cases. On the other hand, when EJC is installed at the exit of TUR, an effective cooling load is produced consequently the required heat exchangers area reduce leading to the lower cost and EI per exergy unit of LNG. This valuable result makes Case II as a convenient configuration for LNG production as compared with Case III. In order to show the advantages of the proposed system, the amounts of produced power and cooling load in the present

Exergoeconomic analysis indicates that 71.0%, 73.5% and 74.21% of the total $\dot{Z}$ are related to LFC in Case I, Case II and Case III, respectively followed by TUR-2 with value of 5.713 \$/h, 5.357 \$/h and 4.831 \$/h in cases I and II and 3.57% in Case III. In most components, the value of $\dot{C}_D$ is dominant. Therefore, the large portion of the cost rates, i.e. $\dot{C}_D + \dot{Z}$, is due to the exergy destruction cost rate of the system. According to the results, the maximum $\dot{C}_D$ and consequently cost rates belong to TST involving 36.45%, 30.59% and 28.76% of total cost rates of the system for Case I, Case II and Case III, respectively. As can be seen, the layouts are compared with those reported in the literature and listed in Table 7. As can be seen, designing the proper configuration for ORC and selecting of suitable refrigerants can improve the amounts of outputs. The cooling load produced in cases I, II and III are 743.1 kJ/s, 1419 kJ/s and 721.3 kJ/s, respectively which are 639.06 kJ/s, 1314.96 kJ/s and 617.26 kJ/s higher than the maximum value reported in [23]. Moreover, the produced power in cases I, II and III are 406.1 kW, 276.5 kW and 293.6 kW higher than the maximum produced power reported by Wang et al.[17]. Tables 8 to 10 present the exergy based results obtained for Case I, Case II and Case III respectively. According to the results, the highest exergy destruction rate belongs to LFC destroying 74.27%, 75.22% and 74.28% of the input exergy in Case I, Case II and Case III, respectively while P-2 has the lowest contribution for destroying the exergy in all cases. The total exergy destruction rate of the system in Case I is 13,588.7 kW while it is about 14,169.6 kW and 13,805 kW in Cases II and III, respectively.

Figure 3. Flow chart of NSGA-II algorithm employed in this research.

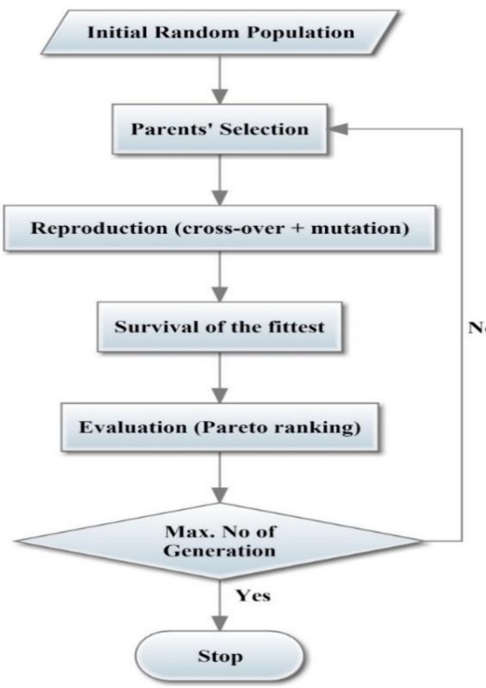

infinite value of r_c in LFC for all cases which is due to the zero value of c_F shows the high potential of this component for reducing the cost rates. The low values of f_c are due to the significant values of $\dot{C}_D$ in components. Comparing the EI results of all cases implies that the maximum component-related EI rate belongs to LFC with values of 4.817 Pts/h for. For this component, EI associated with exergy destruction is zero. Further results show that the remaining components have higher $\dot{B}_D$ in comparison with $\dot{Y}$ and the value of EI rates, i.e. $\dot{Y}+\dot{B}_D$, is affect by $\dot{B}_D$. Among the components, CON-2 with highest value of $\dot{B}_D$ has the maximum contribution in EI rates so that it may dominate 31.6%, 28.33% and 22.08% of total EI rates of the system for Case I, Case II and Case III, respectively. Therefore, this component has a constitutional role in EI formation. The high value of r_b indicate the reducing potential of EI in components. In this manner, LFC has the maximum potential followed by CON-1 for all cases. Due to the high contribution of $\dot{B}_D$ in most components, the value of f_b is little. Therefore, focus should be put on decreasing the irreversibilities.

2.1. Sensitivity study

In this section, the influences of the substantial design parameters, namely mass flow rate of HT ORC loop ($\dot{m}_1$), stabilizer subsystem mass flow rate ($\dot{m}_E$), LNG extracted mass flow rate ($\dot{m}_{G8}$), P-1 inlet pressure (P_1), TUR-1 inlet pressure (P_5), TUR-2 inlet pressure (P_{20}), P-2 inlet pressure (P_{15}), EJC-2 primary pressure (P_{29}) as well as solar irradiation are studied and compared on the performances of the system for Case I and the improved Case II.

2.1.1. Effects of solar irradiation on the performance of the cycles

Figs. 4 and 5 illustrate the influences of the monthly average solar irradiation respectively on the energy and exergy efficiencies of the system for all cases. As a result, the increase of solar irradiation over the first six month causes the reduction in energy and exergy efficiencies because of the slight increase in the outputs so that the cooling effect produced may drop within 2.15% for Case I, 1.66% for Case II, and 2.2% for Case III although the net power increases by about 6.14%, 6.81% and 7.38% for cases I, II and III, respectively. For this manner, the energy efficiency reduces in average 7.9% in Case I, 8.57% in Case II and 7.74% in Case III. As can be seen in Figure 4 and according Figure 5, to, the exergy efficiency of the system drops within 6.7%, 7.65% and 6.35%, respectively, for cases I, II and III. These variations are reversed when the solar irradiation lessens during the second six months. The 42% reduction in solar radiation causes the 5.25% reduction of power produced in Case I, 6.4% decrement in Case II and 6.87% reduction in Case III while the cooling effects increases slightly within 1.99%, 1.69% and 2.2% in cases I, II and III respectively. Referring to Figure 4, the energy efficiency grows by about 17.8%, 9.4% and 15.66% in cases I, II and III, respe ctively and the exergy efficiency increases within 16.6%, 15.4% and 13.96% in cases I, II and III, respectively as shown in Figure 5.

Outcomes indicate that the maximum thermodynamic efficiencies are related to October for all cases so that the energy and exergy efficiencies may increase respectively within 10.48% and 6.421% for Case I, 16.44% and 8.101% for Case II and 8.91% and 5.403% for Case III, respectively. Similar variation trend can be observed for power efficiency of all cases as solar radiation varies during a year. October gives the highest values of power efficiency for all cases so that it may be reaches 3.88%, 3.55% and 3.34% for cases II, III and I, respectively.

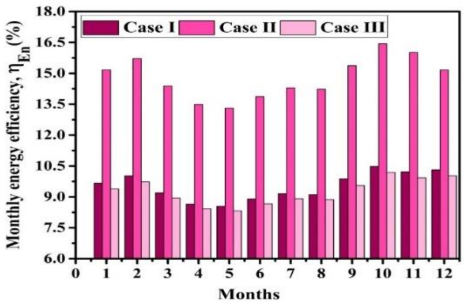

Figure 4. The effects of solar radiation on the energy efficiencies of all cases.

Figure 6 depicts the variations of total product cost rate versus solar irradiation changes. According to the results, the increase of solar radiation reduces the product cost rate of the system for all studied cases. As can be seen, Case III leads to the lowest total cost rate followed by Case II and Case I, respectively. In this manner, the 43% increment in solar radiation from January to June causes 1.08% reduction in TUR-1 product cost rate for Case I and consequently the total product cost rate of system drops

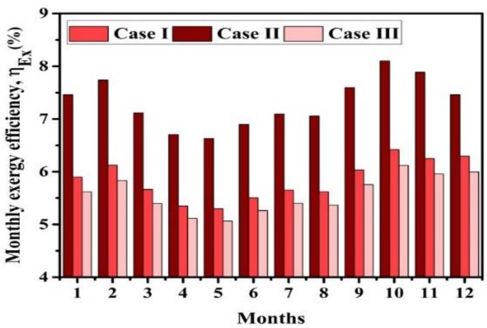

Figure 5. The effects of solar radiation on the exergy efficiencies of all cases

Table 2. Cost and EI balances with corresponding auxiliary equations

Components		Exergoeconomic relations: Cost rate balance	Exergoeconomic relations: Auxiliary equation	Exergoenvironmental relations: EI rate balance	Exergoenvironmental relations: Auxiliary equation
All Cases	LFC	$c_{S3}\dot{E}x_{S3}+c_{sun}\dot{E}x_{sun}+\dot{Z}_{LFC}=c_{S1}\dot{E}x_{S1}$	-	$b_{S3}\dot{E}x_{S3}+b_{sun}\dot{E}x_{sun}+\dot{Y}_{LFC}=b_{S1}\dot{E}x_{S1}$	-
	P-3	$c_{P-3}\dot{W}_{P-3}+c_{S2}\dot{E}x_{S2}+\dot{Z}_{P-3}=c_{S3}\dot{E}x_{S3}$	-	$b_{P-3}\dot{W}_{P-3}+b_{S2}\dot{E}x_{S2}+\dot{Y}_{P-3}=b_{S3}\dot{E}x_{S3}$	-
	TST	$c_{E4}\dot{E}x_{E4}+c_{S1}\dot{E}x_{S1}+\dot{Z}_{TST}=c_{S2}\dot{E}x_{S2}+c_{E1}\dot{E}x_{E1}$	$c_{E1}=c_{S2}$	$b_{E4}\dot{E}x_{E4}+b_{S1}\dot{E}x_{S1}+\dot{Y}_{TST}=b_{S2}\dot{E}x_{S2}+b_{E1}\dot{E}x_{E1}$	$b_{E1}=b_{S2}$
	PRC-1	$c_{G1}\dot{E}x_{G1}+c_2\dot{E}x_2+\dot{Z}_{PRC-1}=c_{G2}\dot{E}x_{G2}+c_3\dot{E}x_3$	$c_2=c_3$	$b_{G1}\dot{E}x_{G1}+b_2\dot{E}x_2+\dot{Y}_{PRC-1}=b_{G2}\dot{E}x_{G2}+b_3\dot{E}x_3$	$b_2=b_3$
	HHE-1	$c_{E1}\dot{E}x_{E1}+c_4\dot{E}x_4+\dot{Z}_{HHE-1}=c_{E2}\dot{E}x_{E2}+c_5\dot{E}x_5$	$c_{E1}=c_{E2}$	$b_{E1}\dot{E}x_{E1}+b_4\dot{E}x_4+\dot{Y}_{HHE-1}=b_{E2}\dot{E}x_{E2}+b_5\dot{E}x_5$	$b_{E1}=b_{E2}$
	HHE-2	$c_{E2}\dot{E}x_{E2}+c_3\dot{E}x_3+\dot{Z}_{HHE-2}=c_{E3}\dot{E}x_{E3}+c_4\dot{E}x_4$	$c_{E2}=c_{E3}$	$b_{E2}\dot{E}x_{E2}+b_3\dot{E}x_3+\dot{Y}_{HHE-2}=b_{E3}\dot{E}x_{E3}+b_4\dot{E}x_4$	$b_{E2}=b_{E3}$
	P-1	$c_{P-1}\dot{W}_{P-1}+c_1\dot{E}x_1+\dot{Z}_{P-1}=c_2\dot{E}x_2$	-	$b_{P-1}\dot{W}_{P-1}+b_1\dot{E}x_1+\dot{Y}_{P-1}=b_2\dot{E}x_2$	-
	CON-1	$c_9\dot{E}x_9+c_{G9}\dot{E}x_{G9}+\dot{Z}_{CON-1}=c_1\dot{E}x_1+c_{G10}\dot{E}x_{G10}$	$c_{G9}=c_{G10}$	$b_9\dot{E}x_9+b_{G9}\dot{E}x_{G9}+\dot{Y}_{CON-1}=b_1\dot{E}x_1+b_{G10}\dot{E}x_{G10}$	$b_{G9}=b_{G10}$
	EVP-1	$c_{G2}\dot{E}x_{G2}+c_{10}\dot{E}x_{10}+\dot{Z}_{EVP-1}=c_{G3}\dot{E}x_{G3}+c_{12}\dot{E}x_{12}$	$c_{10}=c_{12}$	$b_{G2}\dot{E}x_{G2}+b_{10}\dot{E}x_{10}+\dot{Y}_{EVP-1}=b_{G3}\dot{E}x_{G3}+b_{12}\dot{E}x_{12}$	$b_{10}=b_{12}$
	PRC-2	$c_{G3}\dot{E}x_{G3}+c_{16}\dot{E}x_{16}+\dot{Z}_{PRC-2}=c_{17}\dot{E}x_{17}+c_{G4}\dot{E}x_{G4}$	$c_{16}=c_{17}$	$b_{G3}\dot{E}x_{G3}+b_{16}\dot{E}x_{16}+\dot{Y}_{PRC-2}=b_{17}\dot{E}x_{17}+b_{G4}\dot{E}x_{G4}$	$b_{16}=b_{17}$
	P-2	$c_{P-2}\dot{W}_{P-2}+c_{15}\dot{E}x_{15}+\dot{Z}_{P-2}=c_{16}\dot{E}x_{16}$	-	$b_{P-2}\dot{W}_{P-2}+b_{15}\dot{E}x_{15}+\dot{Y}_{P-2}=b_{16}\dot{E}x_{16}$	-
	CON-2	$c_{G8}\dot{E}x_{G8}+c_{23}\dot{E}x_{23}+\dot{Z}_{CON-2}=c_{15}\dot{E}x_{15}+c_{G9}\dot{E}x_{G9}$	$c_{G8}=c_{G9}$	$b_{G8}\dot{E}x_{G8}+b_{23}\dot{E}x_{23}+\dot{Y}_{CON-2}=b_{15}\dot{E}x_{15}+b_{G9}\dot{E}x_{G9}$	$b_{G8}=b_{G9}$
	REG	$c_{17}\dot{E}x_{17}+c_{22}\dot{E}x_{22}+\dot{Z}_{REG}=c_{23}\dot{E}x_{23}+c_{18}\dot{E}x_{18}$	$c_{23}=c_{18}$	$b_{17}\dot{E}x_{17}+b_{22}\dot{E}x_{22}+\dot{Y}_{REG}=b_{23}\dot{E}x_{23}+b_{18}\dot{E}x_{18}$	$b_{17}=b_{18}$
	CHE	$c_7\dot{E}x_7+c_{18}\dot{E}x_{18}+\dot{Z}_{CHE}=c_8\dot{E}x_8+c_{19}\dot{E}x_{19}$	$c_8=c_{19}$	$b_7\dot{E}x_7+b_{18}\dot{E}x_{18}+\dot{Y}_{CHE}=b_8\dot{E}x_8+b_{19}\dot{E}x_{19}$	$b_8=b_{19}$
	LHE-1	$c_{E3}\dot{E}x_{E3}+c_{19}\dot{E}x_{19}+\dot{Z}_{LHE-1}=c_{E4}\dot{E}x_{E4}+c_{20}\dot{E}x_{20}$	$c_{20}=c_{E4}$	$b_{E3}\dot{E}x_{E3}+b_{19}\dot{E}x_{19}+\dot{Y}_{LHE-1}=b_{E4}\dot{E}x_{E4}+b_{20}\dot{E}x_{20}$	$b_{20}=b_{E4}$
	EVP-2	$c_{G5}\dot{E}x_{G5}+c_{25}\dot{E}x_{25}+\dot{Z}_{EVP-2}=c_{26}\dot{E}x_{26}+c_{27}\dot{E}x_{27}$	$c_{25}=c_{27}$	$b_{G5}\dot{E}x_{G5}+b_{25}\dot{E}x_{25}+\dot{Y}_{EVP-2}=b_{26}\dot{E}x_{26}+b_{27}\dot{E}x_{27}$	$b_{25}=b_{27}$
Case I	TUR-1	$c_5\dot{E}x_5+\dot{Z}_{TUR-1}=c_6\dot{E}x_6+c_{14}\dot{E}x_{14}+c_{TUR-1}\dot{W}_{TUR-1}$	$c_5=c_6=c_{14}$	$b_5\dot{E}x_5+\dot{Y}_{TUR-1}=b_6\dot{E}x_6+b_{14}\dot{E}x_{14}+b_{TUR-1}\dot{W}_{TUR-1}$	$b_5=b_6=b_{14}$
	EJC-1	$c_{12}\dot{E}x_{12}+c_{14}\dot{E}x_{14}+\dot{Z}_{EJC-1}=c_{13}\dot{E}x_{13}$	-	$b_{12}\dot{E}x_{12}+b_{14}\dot{E}x_{14}+\dot{Y}_{EJC-1}=b_{13}\dot{E}x_{13}$	-
	TUR-2	$c_{20}\dot{E}x_{20}+\dot{Z}_{TUR-2}=c_{TUR-1}\dot{W}_{TUR-2}+c_{21}\dot{E}x_{21}+c_{29}\dot{E}x_{29}$	$c_{20}=c_{21}=c_{29}$	$b_{20}\dot{E}x_{20}+\dot{Y}_{TUR-2}=b_{TUR-1}\dot{W}_{TUR-2}+b_{21}\dot{E}x_{21}+b_{29}\dot{E}x_{29}$	$b_{20}=b_{21}=b_{29}$
	EJC-2	$c_{27}\dot{E}x_{27}+c_{29}\dot{E}x_{29}+\dot{Z}_{EJC-2}=c_{28}\dot{E}x_{28}$	-	$b_{27}\dot{E}x_{27}+b_{29}\dot{E}x_{29}+\dot{Y}_{EJC-2}=b_{28}\dot{E}x_{28}$	-
Case II	TUR-1	$c_5\dot{E}x_5+\dot{Z}_{TUR-1}=c_6\dot{E}x_6+c_{TUR-1}\dot{W}_{TUR-1}$	$c_5=c_6$	$b_5\dot{E}x_5+\dot{Y}_{TUR-1}=b_6\dot{E}x_6+b_{TUR-1}\dot{W}_{TUR-1}$	$b_5=b_6$
	EJC-1	$c_{12}\dot{E}x_{12}+c_6\dot{E}x_6+\dot{Z}_{EJC-1}=c_7\dot{E}x_7$	-	$b_{12}\dot{E}x_{12}+b_6\dot{E}x_6+\dot{Y}_{EJC-1}=b_7\dot{E}x_7$	-
	TUR-2	$c_{20}\dot{E}x_{20}+\dot{Z}_{TUR-2}=c_{TUR-1}\dot{W}_{TUR-2}+c_{21}\dot{E}x_{21}+c_{29}\dot{E}x_{29}$	$c_{20}=c_{21}=c_{29}$	$b_{20}\dot{E}x_{20}+\dot{Y}_{TUR-2}=b_{TUR-1}\dot{W}_{TUR-2}+b_{21}\dot{E}x_{21}+b_{29}\dot{E}x_{29}$	$b_{20}=b_{21}=b_{29}$
	EJC-2	$c_{27}\dot{E}x_{27}+c_{29}\dot{E}x_{29}+\dot{Z}_{EJC-2}=c_{28}\dot{E}x_{28}$	-	$b_{27}\dot{E}x_{27}+b_{29}\dot{E}x_{29}+\dot{Y}_{EJC-2}=b_{28}\dot{E}x_{28}$	-
Case III	TUR-1	$c_{5'}\dot{E}x_{5'}+\dot{Z}_{TUR-1}=c_6\dot{E}x_6+c_{TUR-1}\dot{W}_{TUR-1}$	$c_{5'}=c_6$	$b_{5'}\dot{E}x_{5'}+\dot{Y}_{TUR-1}=b_6\dot{E}x_6+b_{TUR-1}\dot{W}_{TUR-1}$	$b_{5'}=b_6$
	EJC-1	$c_{12}\dot{E}x_{12}+c_{14}\dot{E}x_{14}+\dot{Z}_{EJC-1}=c_{13}\dot{E}x_{13}$	-	$b_{12}\dot{E}x_{12}+b_{14}\dot{E}x_{14}+\dot{Y}_{EJC-1}=b_{13}\dot{E}x_{13}$	-
	TUR-2	$c_{20'}\dot{E}x_{20'}+\dot{Z}_{TUR-2}=c_{TUR-1}\dot{W}_{TUR-2}+c_{21}\dot{E}x_{21}$	$c_{20'}=c_{21}$	$b_{20'}\dot{E}x_{20'}+\dot{Y}_{TUR-2}=b_{TUR-1}\dot{W}_{TUR-2}+b_{21}\dot{E}x_{21}$	$b_{20'}=b_{21}$
	EJC-2	$c_{27}\dot{E}x_{27}+c_{29}\dot{E}x_{29}+\dot{Z}_{EJC-2}=c_{28}\dot{E}x_{28}$	-	$b_{27}\dot{E}x_{27}+b_{29}\dot{E}x_{29}+\dot{Y}_{EJC-2}=b_{28}\dot{E}x_{28}$	-

Table 3. Optimization constraints and their reasons.

Decision variable	Case I		Case II		Rationale
	Lower	Upper	Lower	Upper	
Both cases					
HT loop mass flow rate, $\dot{m}_1$ (kg/s)	10	12	10	12	P-1 required power limitation
Stabilizer subsystem mass flow rate, $\dot{m}_E$ (kg/s)	30	32	31.2	33	Input energy limitation
LNG extracted mass flow rate, $\dot{m}_{G8}$ (kg/s)	17	18.5	22	28.8	CONs required energy limitation
P-1 inlet pressure, P_1 (kPa)	120	250	120	250	TUR-1 commercial availability
EJC-1 suction pressure, P_{12} (kPa)	15	20	15	20	EJC-1 operating limit
TUR-1 inlet pressure, P_5 (kPa)	1100	2000	1792	2900	TUR-1 commercial availability
EJC-2 primary pressure, P_{29} (kPa)	500	900	500	900	EJC-2 operating limit
P-2 inlet pressure, P_{15} (kPa)	120	174	70	135	TUR-2 commercial availability
TUR-2 inlet pressure, P_{20} (kPa)	765	850	765	850	TUR-2 commercial availability
Case I					
EJC-1 primary pressure, P_{14} (kPa)	400	1100	-	-	EJC-1 operating limit

Table 4. Genetic algorithm parameters.

Parameter	Value
Population size	200
Generation size	100
Crossover fraction	0.8
Mutation rate	0.01
Selection process	Tournament

Table 5. Input data for all cases.

Term	Value		
	Case I	Case II	Case III
Annual solar irradiation, H (kWh/m^2.day)	7.35	7.35	7.35
TUR-1 inlet pressure, P_5 (kPa)	2400	2400	2400
TUR-2 inlet pressure, P_{20} (kPa)	800	800	800
TUR-1 outlet pressure, P_6 (kPa)	150	150	150
TUR-2 outlet pressure, P_{21} (kPa)	120	120	120
Solar subsystem pressure, P_E (kPa)	105	105	105
Inlet temperature of solar subsystem, T_{E4} (K)	325	325	325
ST mass flow rate, $\dot{m}_E$ (kg/s)	30	32.8	30
EJC-2 outlet pressure, P_{28} (kPa)	100	100	100
EJC-1 primary pressure, P_{12} (kPa)	16	16	16
EJC-2 primary pressure, P_{27} (kPa)	8	8	8
NG pressure, P_{G1} (kPa)	3500	3500	3500
NG inlet temperature , T_{G1} (K)	300	300	300
Mass flow rate of NG, $\dot{m}_{G1}$ (kg/s)	2	4	2
HT loop mass flow rate, $\dot{m}_1$ (kg/s)	12	12	12
P-3 outlet pressure, P_{S3} (kPa)	500	500	500
Mass flow rate of bottom cycle, $\dot{m}_{16}$ (kg/s)	7.3	9	7.3

Table 6. The results obtained at the design point for all studied cases

Performance	Case I	Case II	Case III
Net power output, $\dot{W}_{net}$ (kW)	520.2	390.6	407.7
Power efficiency, η_{Power} (kW)	4.11%	3.09%	3.22%
Annual energy efficiency, η_{En} (%)	9.984	14.3	8.922
Annual exergy efficiency, η_{Ex} (%)	6.482	7.101	5.411
Total product cost rate, $\dot{C}_P^{tot}$ ($/h)	80.82	79.92	78.372
Total EI rate, $\dot{B}_P^{tot}$ (Pts/h)	78.228	96.912	79.272
Mass flow rate of LNG, $\dot{m}_{LNG}$ (kg/s)	2	4	2
Cost per exergy unit of LNG, c_{LNG} ($/GJ)	0.429	0.426	0.435
EI per exergy unit of LNG, b_{LNG} (Pts/GJ)	7.367	7.35	7.373

Table 7. Comparison of present configurations with those reported in the literature.

Cycle proposed		ORC type		Cooling load (kJ/s)	Produced power (kW)
		Single/refrigerant	Cascade/refrigerant		
In present work	Case I	-	R227ea, R32	743.1	520.2
	Case II	-	R227ea, R32	1419	390.6
	Case III	-	R227ea, R32	721.3	407.7
by Wang et al.[17]		R123	-	21.01	114.1
by Zheng and Weng [46]		R245fa	-	19.39	27.9
by Ahmadzadeh et al.[20]		R141b	-	9.35	49.9
by Ahmadzadeh et al. [20]		R123	-	15.74	21.43
by Rostamzadeh et al.[22]		Butene	-	98.49	53.44
by Ebadollaet al.[23]		R113	-	104.04	49.82

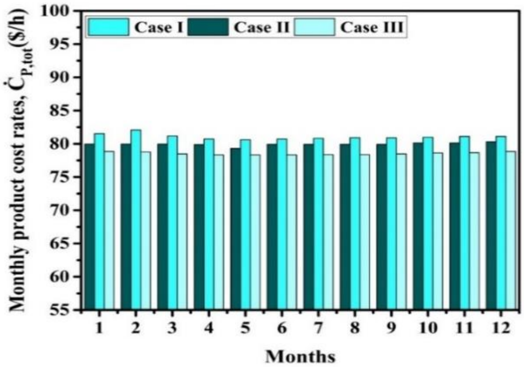

Figure 6. The effects of solar radiation on the total product cost rate of all cases

within 1.14%. The same trend is observed for Cases II and III with 0.8% and 0.91% decrements in the total product cost rate. During the last six months of the year as the solar radiation increases the total product cost rate increases within 0.94% for Case I, by about 0.18% and 0.63 % for Case II and Case III due to the negative impact of TUR-1 product cost rate. On the contrary, when solar radiation increases during the first six months, the temperature of point E1 increases improving the operation of HTH and reducing its area. Therefore, the total investment cost of the system lessens. According to these variations and exergy reduction of G7, the cost per exergy unit of LNG drops. This trend is reversed over June to December. In this manner, the required heat transfer area for providing TURs entrance energies increases which causes the increment in the total investment cost rate of the system.

According to Figure 6, these changes increase the cost per exergy unit of LNG within 0.9% for Case I, 0.4% for Case II and 0.9% for Case III. Although Case III gives the lowest total cost rate, the cost per unit exergy of LNG gets maximum in this layout while it is the lowest value in Case II as can be seen in Figure 7. Figure 8 implies the effects of solar irradiation on the total EI rate of the system for all cases. According to the results, the increase of solar irradiation from January to June affects the total EI of the system, negatively due to increases of TURs product EI rates. In this case, the total EI

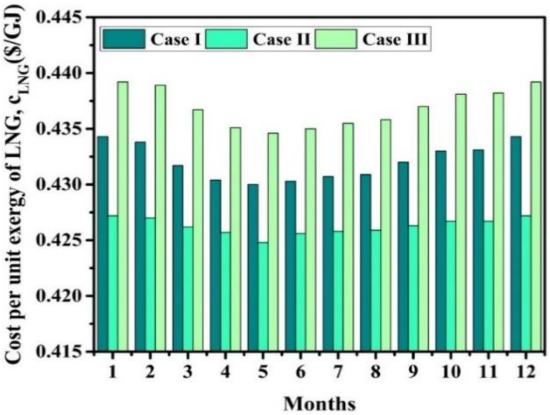

Figure 7. The effects of solar radiation on the cost per exergy unit of LNG for all cases

rate of the system increases within 1.9% for Case I, 1.8% for Case II and 2.08% for Case III. The reduction of solar irradiation from June to December reduces the total EI rate of the system by about 1.9% for Case I, 1.7% for Case II and 2.04% for Case III. Although the EI rate of Case II is higher than that of Case I, the EI per exergy unit of LNG in Case II is lower than that of Case I within 0.01 Pts/GJ while it is almost the same in Case I and III. As can be seen, Moreover, the solar irradiation does not have a drastic influence on the EI per exergy unit of LNG for all cases.

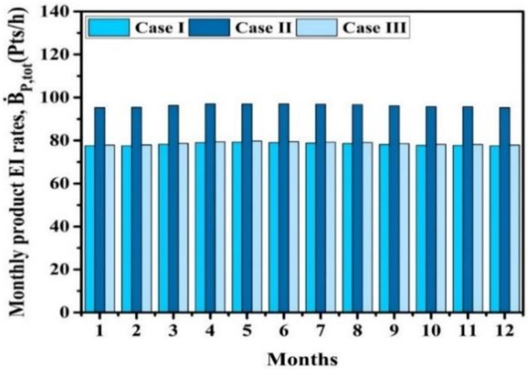

Figure 8. The effects of solar radiation on the product EI rate of all cases

2.1.2. Effects of major parameters on the annual energy and exergy efficiencies

Sensitivity analysis shows that P_1, P_{15}, P_{12}, P_{29} affect the efficiencies of all cases, negatively and the increase of P_{29} from 500 kPa to 900 kPa has the maximum reduction effects so that energy and exergy efficiencies of system may reduce within 7.34% and 11.7% for Case I, about 6.4% and 12.3% for Case II and 6.98% and 8.96% for Case III, respectively. These decrements are due the decrease of TUR-2 power output caused by the EJC-2 primary pressure increment. The thermodynamic performances of the system in Case I and Case III depend on P_1 variation, as P_1 increases from 120 kPa to 250 kPa, the energy and exergy efficiencies lessen slightly within 2.3% and 3.67% for Case I and 3.1% and 4.12% for Case III, respectively while the efficiencies of the system for Case II are not affected by the increase of P_1. The negative influence of P_{15} on efficiencies of the system for cases I and II are lower than 2% while the energy and exergy of Case III reduce 3.95% and 5.28%, respectively. Moreover, P_{12} with the lowest decrements on efficiencies (lower than 1%) is in the last ranking.

The remaining parameters affect the efficiencies, positively. Figs. 9 and 10 show the effects of $\dot{m}_1$ and $\dot{m}_{G8}$ on the efficiencies of the system for all cases. According to the results, the increase of $\dot{m}_1$ from 10 kg/s to 12 kg/s rises the power produced by HT ORC loop for all cases. Therefore, the energy efficiency increases for all cases. Case I gives the maximum range of 3.95%-4.11% followed by cases III and II, respectively with ranges of 3.1%-3.22% and 2.97%-3.08%, respectively. Moreover, the energy efficiencies of the system increase respectively

Table 8. Thermodynamic, exergy, exergoeconomic, exergoenvironmental impact analyses for the material streams for Case II.

State	Fluid	Thermodynamic data					Exergy analysis				Exergoeconomic analysis			Exergoenvironment analysis		
		T (K)	P (kPa)	$\dot{m}$ (kg/s)	h (kJ/kg)	s (kJ/kgK)	$\dot{E}x^{Ph}$ (MW)	$\dot{E}x^{T}$ (MW)	$\dot{E}x^{M}$ (MW)	$\dot{E}x^{ch}$ (MW)	$\dot{C}^{Ph}$ (\$/h)	$\dot{C}^{ch}$ (\$/h)	c (\$/GJ)	$\dot{B}^{Ph}$ (Pts/h)	$\dot{B}^{ch}$ (Pts/h)	b (Pts/GJ)
E1	Therminol_VP1	391.6	105	32.8	178.5	0.5288	0.6641	-	-	-	57.69	-	24.13	7.719	-	3.229
E2	Therminol_VP1	377.2	105	32.8	152.2	0.4604	0.4749	-	-	-	41.25	-	24.13	5.520	-	3.229
E3	Therminol_VP1	355.8	105	32.8	113.1	0.3538	0.2428	-	-	-	21.09	-	24.13	2.822	-	3.229
E4	Therminol_VP1	325	105	32.8	56.72	0.188	0.0242	-	-	-	2.01	-	23.03	2.014	-	23.13
S1	Therminol_VP1	522.3	105	32.8	440.4	1.104	3.597	-	-	-	110.9	-	8.566	13.41	-	1.036
S2	Therminol_VP1	391.6	105	32.8	178.5	0.5288	0.6641	-	-	-	57.69	-	24.13	7.719	-	3.229
S3	Therminol_VP1	391.8	500	32.8	178.9	0.5299	0.6673	-	-	-	59.67	-	24.84	8.604	-	3.582
G1	NG	300	3500	4	-30.37	-1.907	2.168	0	2.168	206.1	3.083	293	0.395	56.90	5409.3	7.291
G2	NG	277.3	3500	4	-86.23	-2.1	2.177	0.0089	2.168	206.1	3.107	294	0.3965	57.16	5411.5	7.294
G3	NG	238.1	3500	4	-185.7	-2.487	2.243	0.0755	2.167	206.1	3.365	309	0.4167	59.09	5430.1	7.319
G4	NG	227.1	3500	4	-215.4	-2.615	2.278	0.1100	2.168	206.1	3.424	310	0.4175	60.03	5430.8	7.32
G5	NG	187.3	3500	26	-350.1	-3.273	16	-	-	1340	24.45	2050	0.4245	423.13	35437.1	7.346
G6	NG	181.9	3500	26	-385.2	-3.464	17	2.919	14.08	1340	26.06	2050	0.4258	449.82	35456.4	7.35
G7	NG	181.9	3500	4	-385.2	-3.464	2.617	0.4491	2.168	206.1	4.012	316	0.4258	69.25	5453.1	7.35
G8	NG	181.9	3500	22	-612.8	-4.715	18	5.720	12.28	1133	27.59	1740	0.4258	476.28	29979.2	7.35
G9	NG	181.9	3500	22	-402.4	-3.558	15	2.715	12.28	1133	22.99	1740	0.4258	396.9	29979.2	7.35
G10	NG	183.2	3500	22	-374.6	-3.405	15	2.319	12.68	1133	22.99	1740	0.4258	396.9	29979.2	7.35
1	R227ea	266.4	150	12	12.42	0.04761	0.2782	0.2115	0.0668	-	11.19	-	11.17	24.88	-	24.84
2	R227ea	267.3	2400	12	14.01	0.04792	0.2962	-	-	-	13.88	-	13.02	26.10	-	24.48
3	R227ea	284.1	2400	12	32.63	0.1155	0.2764	-	-	-	12.95	-	13.02	24.36	-	24.48
4	R227ea	365.1	2400	12	139.3	0.4431	0.3777	-	-	-	33.63	-	24.73	27.19	-	20
5	R227ea	379.6	2400	12	211.2	0.6385	0.5362	-	-	-	50.79	-	26.31	29.59	-	15.33
6	R227ea	345.9	800	12	198.7	0.6449	0.3637	-	-	-	34.45	-	26.31	20.07	-	15.33
7	R227ea	295.3	150	20.31	162.9	0.6079	0.1136	-	-	-	26.61	-	65.07	9.411	-	23.01
8	R227ea	266.4	150	20.31	63.37	0.2388	0.3409	0.2279	0.113	-	17.88	-	14.57	24.36	-	19.85
9	R227ea	266.4	150	12	63.37	0.2388	0.2014	0.1346	0.0667	-	10.56	-	14.57	14.39	-	19.85
10	R227ea	266.4	150	8.315	63.37	0.2388	0.1395	0.0933	0.0462	-	7.32	-	14.57	9.969	-	19.85
11	R227ea	221.3	16	8.315	63.37	0.2978	-0.0076	0.2147	-0.2224	-	-	-	-	-	-	-
12	R227ea	221.3	16	8.315	111.2	0.514	-0.1492	0.0732	-0.2224	-	-7.83	-	14.57	-10.66	-	19.85
15	R32	224	120	9	120	0.6805	1.295	-	-	-	7.384	-	1.58	69.37	-	14.88
16	R32	225.1	800	9	120.6	0.6805	1.300	0.4458	0.8544	-	8.190	-	1.75	69.96	-	14.95
17	R32	233.4	800	9	133.8	0.7383	1.264	0.4091	0.8544	-	7.963	-	1.75	68.03	-	14.95
18	R32	272.6	800	9	146.7	0.8902	1.233	0.3783	0.8544	-	42.76	-	9.63	86.02	-	19.38
19	R32	272.6	800	9	371.4	1.629	0.9980	0.1436	0.8544	-	52.35	-	14.57	71.32	-	19.85
20	R32	331.1	800	9	577	2.362	0.8680	-	-	-	71.96	-	23.03	72.28	-	23.13
21	R32	317.2	120	4.5	576.2	2.653	0.0378	-	-	-	3.139	-	23.03	3.153	-	23.13
22	R32	262.5	120	11.58	529.9	2.493	0.1170	0.0247	0.0927	-	39.43	-	93.37	27.55	-	65.25
23	R32	250.4	120	11.58	519.8	2.454	0.1370	0.0445	0.0927	-	47.58	-	96.34	9.572	-	19.38
24	R32	224.9	120	11.58	120	0.6805	1.667	1.223	0.4440	-	9.51	-	1.584	89.29	-	14.88
25	R32	224.9	120	2.581	120	0.6805	0.3710	-	-	-	2.12	-	1.584	19.89	-	14.88
26	R32	180.9	8	2.581	120	0.7191	0.3410	0.6543	-0.3128	-	-	-	-	-	-	-
27	R32	180.9	8	2.581	473.8	2.665	-0.2520	0.0611	-0.3128	-	-1.43	-	1.584	-13.48	-	14.88
28	R32	226.1	120	7.081	500.5	2.401	0.0596	-	-	-	36.29	-	169.1	2.441	-	11.37
29	R32	325.2	900	4.5	515.8	2.443	0.4550	-	-	-	37.73	-	23.03	37.89	-	23.13

Table 9. Thermodynamic, exergy, exergoeconomic, exergoenvironmental impact analyses for the material streams for Case III.

State	Fluid	Thermodynamic data					Exergy analysis				Exergoeconomic analysis			Exergoenvironment analysis		
		T (K)	P (kPa)	$\dot{m}$ (kg/s)	h (kJ/kg)	s (kJ/kgK)	$\dot{E}x^{Ph}$ (MW)	$\dot{E}x^{T}$ (MW)	$\dot{E}x^{M}$ (MW)	$\dot{E}x^{ch}$ (MW)	$\dot{C}^{Ph}$ (\$/h)	$\dot{C}^{ch}$ (\$/h)	c (\$/GJ)	$\dot{B}^{Ph}$ (Pts/h)	$\dot{B}^{ch}$ (Pts/h)	b (Pts/GJ)
E1	Therminol_VP1	392.2	105	30	179.7	0.532	0.616	-	-	-	57.74	-	26.06	7.74	-	3.491
E2	Therminol_VP1	376.3	105	30	150.6	0.456	0.424	-	-	-	39.81	-	26.06	5.33	-	3.491
E3	Therminol_VP1	351	105	30	104.2	0.329	0.181	-	-	-	16.99	-	26.06	2.28	-	3.491
E4	Therminol_VP1	325	105	30	56.6	0.188	0.021	-	-	-	2.029	-	26.54	2.00	-	26.19
S1	Therminol_VP1	535.1	105	30	468.7	1.157	3.660	-	-	-	111.0	-	8.425	13.47	-	1.022
S2	Therminol_VP1	392.2	105	30	179.7	0.532	0.616	-	-	-	57.74	-	26.06	7.74	-	3.491
S3	Therminol_VP1	392.4	500	30	180.1	0.533	0.619	-	-	-	59.76	-	26.84	8.65	-	3.885
G1	NG	300	3500	2	-30.4	-1.907	1.083	-	1.083	103	1.540	147	0.395	28.43	2705	7.291
G2	NG	277.3	3500	2	-86.2	-2.100	1.088	0.004	1.084	103	1.555	147	0.3971	28.57	2706	7.294
G3	NG	241.4	3500	2	-177.0	-2.451	1.117	0.033	1.084	103	1.688	156	0.4197	29.44	2716	7.321
G4	NG	230.1	3500	2	-207.2	-2.579	1.133	0.050	1.083	103	1.714	156	0.4203	29.87	2717	7.323
G5	NG	186.8	3500	20	-352.3	-3.285	13.00			1030	20.31	1609	0.4339	344.8	27321	7.368
G6	NG	181.9	3500	20	-391.0	-3.496	14.00	2.321	11.679	1030	21.94	1614	0.4354	371.6	27339	7.373
G7	NG	181.9	3500	2	-391.0	-3.496	1.315	0.232	1.083	103	2.061	162	0.4354	34.90	2735	7.373
G8	NG	181.9	3500	18	-612.8	-4.715	14.43	4.680	9.754	927	22.62	1454	0.4354	383.1	24616	7.373
G9	NG	181.9	3500	18	-402.4	-3.558	11.98	2.222	9.754	927	18.77	1454	0.4354	317.9	24616	7.373
G10	NG	184.1	3500	18	-368.4	-3.372	11.58	1.828	9.754	927	18.15	1454	0.4354	307.4	24616	7.373
1	R227ea	266.4	150	12	12.4	0.048	0.278	0.212	0.067	-	13.63	-	13.61	27.02	-	26.98
2	R227ea	267.3	2400	12	14.0	0.048	0.296	-	-	-	16.61	-	15.58	28.40	-	26.63
3	R227ea	275.8	2400	12	23.3	0.082	0.284	-	-	-	15.95	-	15.58	27.26	-	26.63
4	R227ea	365.1	2400	12	139.3	0.443	0.378	-	-	-	39.28	-	28.89	30.46	-	22.40
5	R227ea	380.2	2400	12	212.0	0.641	0.538	-	-	-	57.97	-	29.91	33.09	-	17.07
5'	R227ea	380.2	2400	6	212.0	0.641	0.269	-	-	-	28.99	-	29.91	16.54	-	17.07
6	R227ea	314.3	150	6	178.7	0.660	0.035	-	-	-	3.772	-	29.91	2.15	-	17.07
7	R227ea	310	150	15.8	175.2	0.648	0.090	-	-	-	28.37	-	87.54	13.10	-	40.43
8	R227ea	266.4	150	15.8	63.4	0.239	0.265	0.177	0.088	-	17.09	-	17.91	21.77	-	22.81
9	R227ea	266.4	150	12.0	63.4	0.239	0.201	0.135	0.067	-	12.99	-	17.91	16.54	-	22.81
10	R227ea	266.4	150	3.79	63.4	0.239	0.064	0.043	0.021	-	4.106	-	17.91	5.23	-	22.81
11	R227ea	221.3	16	3.79	111.2	0.298	-0.003	0.098	-0.102	-	-	-	-	-	-	-
12	R32	221.3	16	3.79	111.2	0.514	-0.068	0.033	-0.102	-	-69.12	-	282	-5.59	-	22.81
13	R32	306.9	150	9.79	173.0	0.652	0.024	-	-	-	2.609	-	29.91	10.96	-	125.6
14	R32	380.2	2400	6.00	212.0	0.641	0.269	-	-	-	1.663	-	1.716	16.54	-	17.07
15	R32	224.9	120	7.30	120.0	0.681	1.365	0.992	0.373	-	8.432	-	1.716	73.71	-	15.00
16	R32	225.1	800	7.30	120.6	0.681	1.055	0.362	0.693	-	7.190	-	1.893	57.24	-	15.07
17	R32	230.3	800	7.30	128.8	0.717	1.035	0.342	0.693	-	7.053	-	1.893	56.15	-	15.07
18	R32	272.6	800	7.30	138.7	0.890	1.015	0.322	0.693	-	39.94	-	10.93	74.43	-	20.37
19	R32	272.6	800	7.30	380.5	1.662	0.803	0.110	0.693	-	51.76	-	17.91	65.92	-	22.81
20	R32	330.1	800	7.30	576.1	2.359	0.703	-	-	-	67.21	-	26.54	66.32	-	26.19
20'	R32	330.1	800	3.65	576.1	2.359	0.352	-	-	-	33.60	-	26.54	33.16	-	26.19
21	R32	237.8	120	3.65	509.3	2.410	0.052	-	-	-	4.975	-	26.54	4.91	-	26.19
22	R32	258.8	120	9.49	526.8	2.481	0.101	0.025	0.076	-	37.27	-	102.9	26.55	-	73.32
23	R32	249.7	120	9.49	519.2	2.451	0.114	0.038	0.076	-	4.466	-	10.93	8.32	-	20.37
24	R32	224.9	120	9.49	120.0	0.681	0.114	-	-	-	4.466	-	10.93	8.32	-	20.37
25	R32	224.9	120	2.19	120.0	0.681	0.315	-	-	-	1.944	-	1.716	16.99	-	15.00
26	R32	181.9	8	2.19	120.0	0.719	0.289	0.555	-0.265	-	-	-	-	-	-	-
27	R32	181.9	8	2.19	473.8	2.665	-0.213	0.052	-0.265	-	-1.318	-	1.716	-11.52	-	15.00
28	R32	271.3	120	5.84	537.7	2.551	0.003	-	-	-	32.28	-	2568	21.65	-	1722
29	R32	330.1	800	3.65	576.1	2.359	0.352	-	-	-	33.60	-	26.54	33.16	-	26.19

Table 10. Comparison of present configurations with those reported in the literature.

Cycle proposed		ORC type		Cooling load (kJ/s)	Produced power (kW)
		Single/refrigerant	Cascade/refrigerant		
In present work	Case I	-	R227ea, R32	743.1	520.2
	Case II	-	R227ea, R32	1419	390.6
	Case III	-	R227ea, R32	721.3	407.7
by Wang et al.[17]		R123	-	21.01	114.1
by Zheng and Weng [45]		R245fa	-	19.39	27.9
by Ahmadzadeh et al.[20]		R141b	-	9.35	49.9
by Ahmadzadeh et al. [20]		R123	-	15.74	21.43
by Rostamzadeh et al.[22]		Butene	-	98.49	53.44
by Ebadollahi et al.[23]		R113	-	104.04	49.82

about 1.76%, 1% and 1.66% for Cases I, II and III, respectively as shown in Figure 9 and according to Figure 10, their exergy efficiencies increase within 2.86%, 1.94% and 2.88%, respectively. A 1.5 kg/s increment of $\dot{m}_{G8}$ affects the efficiencies positively due to the exergy destruction reduction. The highest increment of energy efficiency is related to Case I with value of 3% while the maximum exergy efficiency belongs to Case III by 2.17%. The power efficiency of the cases does not affected by variation of this parameter.

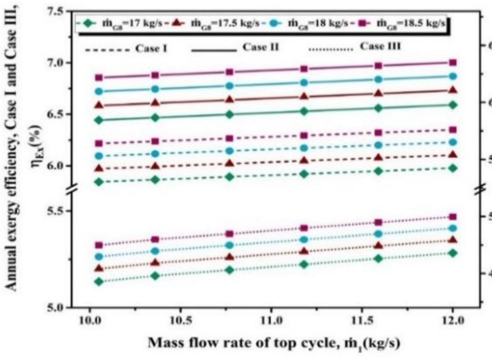

Figure 9. The effects of HT ORC mass flow rate on the annual energy efficiencies

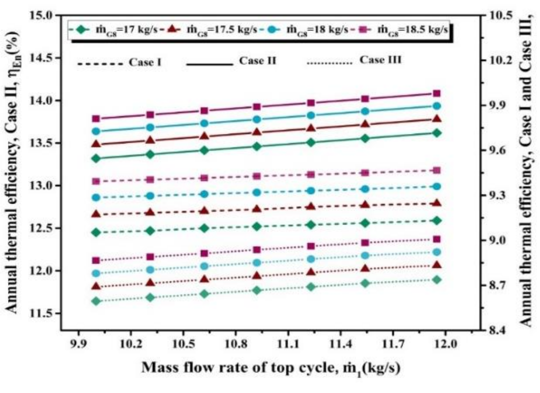

Figure 10. The effects of HT ORC and LNG extraction mass flow rates on the annual exergy efficiencies

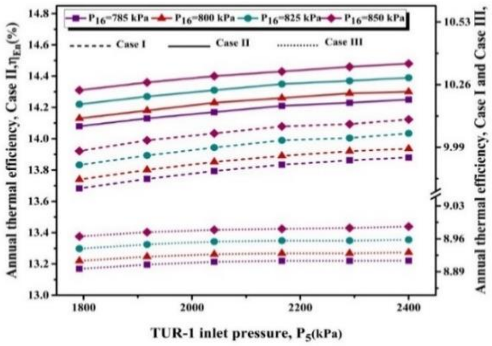

Figure 11. The effects of TURs-1 and 2 inlet pressures on the annual energy efficiencies

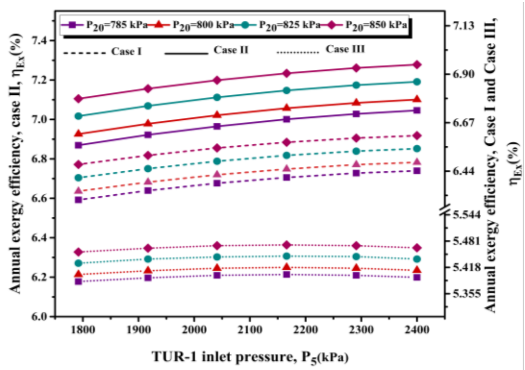

Figure 12. The effects of TURs-1 and 2 inlet pressures on the annual exergy efficiencies

Figs. 11 and 12 illustrate the impacts of P_5 and P_{20} increments on the energy and exergy efficiencies, respectively of the system for all cases studied. According to the results, the variations of P_{20} from 785 kPa to 850 kPa on the efficiencies are higher than P_5 due to the increase of power produced and the exergy efficiencies are improved more than energy efficiencies for all cases as P_5 and P_{20} grow. According to Figure 11, the increase trend of energy efficiency of Case I with a value of 1.35% is higher than that of Case II and Case III with values of 1.2% and 0.11% as P_5 grows while the increase of energy efficiencies are the same for cases I and II and it is about 0.77% for Case III as P_{20} increases. Moreover, the highest range of power efficiency is related to Case I by 3.99%-4.11% while its maximum increment belongs to Case II by 5% as P_5 increases. Similar increment trend can be obtained for power efficiencies when P_{16} increases. In this manner, the maximum increase in power efficiency with a value of 8.5% is obtained for Case I with the highest range of 4.03%-4.22% followed by cases I and III with values of 4.7% and 2.5%, respectively. Figure 12 implies that in Case II exergy efficiencies are improved better than those of Case I and Case III when P_5 and P_{20} grow so that the exergy efficiency of Case II can increase within 4.42% with P_{20} increment.

Among the parameters, the slight variation of $\dot{m}_E$ from 31.2 kg/s to 32 kg/s has the lowest positive effect on the efficiencies due to the little increase in TUR-1 inlet temperature.

2.1.3. *Effects of major parameters on the total product cost rate of cycle*

Parametric study indicates that P_{20}, P_5, $\dot{m}_1$ and $\dot{m}_{G8}$ cause the increments in total product cost rate for all cases so that $\dot{m}_{G8}$ growth may have the highest negative effect on the cost rate of Case I within 3.23% followed by Case III with 2.65% while P_5 affects the cost rate of Case II drastically by about 1.5% among the parameters with negative effects due to the cost rate of produced power. The lowest increments for Case I (<0.5%) and Case II (0.36%) are obtained when P_5 and $\dot{m}_{G8}$ grow, respectively. P_{20} has the lowest negative effect of the cost rate of Case III (<0.37%). Outcomes also indicate that P_{12}, P_{29} and P_{15} increments lead to the improvements in total product cost rates of all cases. P_{12} has a little positive effect on the total product cost rate of all cases within 0.09% because of the slight reduction in the exergy destruction cost rate of the system.

Figure 13 shows the effects of P_1 and $\dot{m}_E$ on the total product cost rate of the system for all cases. As clarity observed, increase of P_1 from 140 kPa to 150 kPa improves Case I and Case III economically within 0.108 \$/h and 0.18 \$/h due to the decrement in exergy destruction while it affects the economic criterion of Case II, negatively (about 0.216 \$/h).

On the contrary, the 0.8 kg/s growth of $\dot{m}_E$ increases the economic performance of Case I by about 0.85% while the total On the contrary, the 0.8 kg/s growth of $\dot{m}_E$ increases the economic performance of Case I by about 0.85% while the total product cost reduces in Case II and Case III within 0.396 \$/h and 0.216 \$/h due to the exergy destruction decrement.

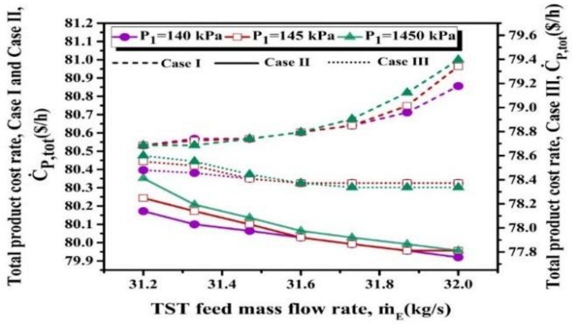

Figure 13. The effects of TST feed mass flow rate and P-1 inlet pressure on the total product cost rate

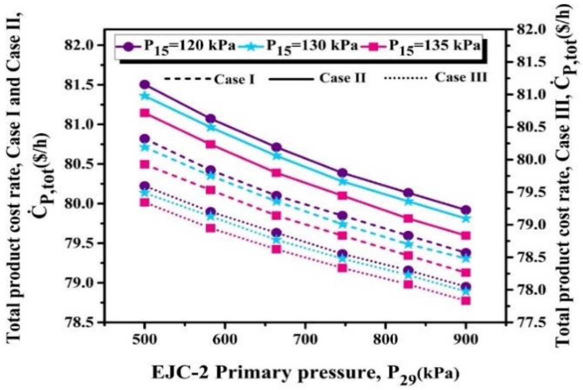

Figure 14. The effects of EJC-2 primary pressure and P-2 inlet pressure on the total product cost rate.

2.1.4. *The effect of major parameters on the total product EI rate*

According to the results, all parameters expect P_{20} have incremental trends on the total product EI rate. The increase of $\dot{m}_{G8}$ from 17 kg/s to 18.5 kg/s, leads to the highest negative effect on the EI within 3.03% for Case I, 2.2% for Case II and 2.65% for Case III due to the increase of EI rate associated with the exergy destruction. In the next rank, P_{29} increment from 500 kPa to 900 kPa affects the EI rate of products negatively within 1.7% for cases I and II and 1.6% for Case III while remaining parameters have slight influence lower than 1%.

Figure 15 illustrates the effects of P_{20} growth on the total EI rate of the system. When P_{20} is supposed to change from 765 kPa to 850 kPa, the EI associated with the total exergy destruction rate reduces and since this decrement in Case II is higher than that of Case I, the total product EI rate is improved within 0.44% and 0.28% in cases II and I, respectively and it remains almost constant in Case III.

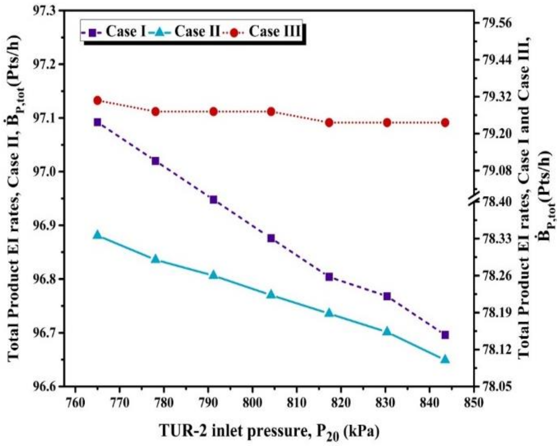

Figure 15. The effects of TUR-2 inlet pressure on the total product EI rate

Optimization results

Figure 16 indicates the 3D Pareto frontier obtained from NSGA-II algorithm and the final optimum solutions identified by LINMAP, TOPSIS and Shannon Entropy decision makers for objectives of cases I and II. The corresponding specified options of Figure 16 are tabulated in Tables 10 and 11.

To identify the reasonable status of different answers obtained through the decision makers, the deviation index (*DI*) of each answer from the ideal one is calculated using Eq. (43) [45].

$$DI = \frac{\sqrt{\sum_{i=1}^{4}\left(F_i - F_i^{ideal}\right)^2}}{\sqrt{\sum_{i=1}^{4}\left(F_i - F_i^{ideal}\right)^2} + \sqrt{\sum_{i=1}^{4}\left(F_i - F_i^{nadir}\right)^2}} \quad (43)$$

Here, F_i is the *i*th objective function. The superscripts "*ideal*" and "*nadir*" refer to the single objective optimization for ideal and non-ideal cases, respectively.

According to Tables 11 and 12, the lowest *DI* with values of 0.1318 and 0.2032 for Case I and Case II, respectively, are related to the LINMAP procedure indicating the highest reliability for the final optimum solutions. In this manner, the maximum improvements in total product cost and EI rates for Case I are calculated within 1.2% and 1.05%, respectively as compared with the base point. For this configuration, the maximum improvements for energy and exergy efficiencies are obtained within 7.37% and 12.63, respectively through Shannon Entropy solution which leads to the lowest reliability. Based upon this, P_{12} and $\dot{m}_E$ with values of 120.1 kPa, 408.5 kPa, 17.56 kPa and 31.53 kg/s, respectively in comparison with other methods are required.

In Case II, although the reliable solution belongs to the LINMAP decision making, the highest improvements of objective functions is only related to the total product cost rate with a value of 2.2%. In this regard, lower P_{20}, P_{15}, P_5 and P_1 with values of 488.6 kPa, 70 kPa, 2031 kPa and 120 kPa, respectively are needed.

For this configuration, the lowest total product EI rate with value of 94.068 (Pts/h) is achieved using Shannon Entropy procedure and the best energy and exergy efficiencies with the maximum increments of 11.67% and 24.02%, respectively are obtained through TOPSIS decision maker.

Table 13 shows the specified options of the system for both configurations. Comparing the results at optimum solutions shows that the power produced in Case I increases within 20.45% leading to the maximum power efficiency of 4.95% through LINMAP procedure while it increases by about 47.31% though TOPSIS for Case II. Although the produced power in Case II is lower than that of Case I about 129.6 kW, the twice mass flow rate of LNG makes it more effective. Moreover, at optimum conditions, the total product cost rate of Case II is worsened so that the maximum increment may be obtained within 2.5% through TOPSIS decision making.

As is clear, the values of cost and EI per exergy unit of LNG at the base point for Case II are improved within 0.7% and 0.23%, respectively. According to the results, the highest decrements in the cost and EI per exergy unit of LNG for Case II are obtained using Shannon Entropy and LINMAP methods by about 0.014 \$/GJ and 0.033 Pts/GJ in relation to the base case.

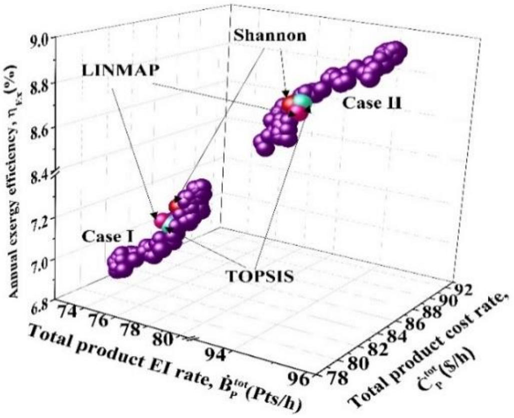

a) Exergy efficiency and total product cost and EI rates

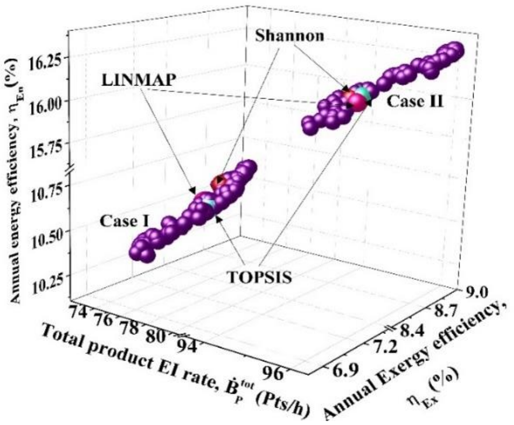

c) Total product cost rate and efficiencies

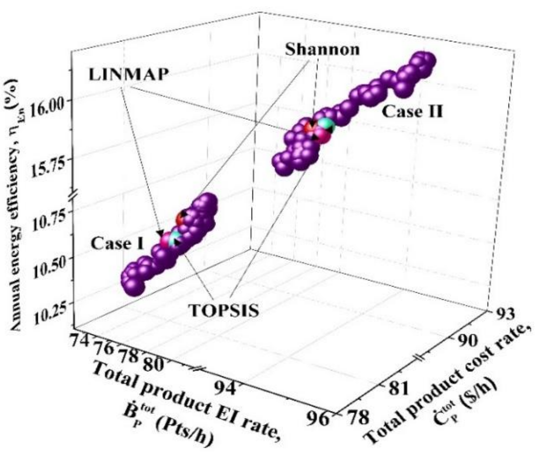

b) Energy efficiency and total product cost and EI rates

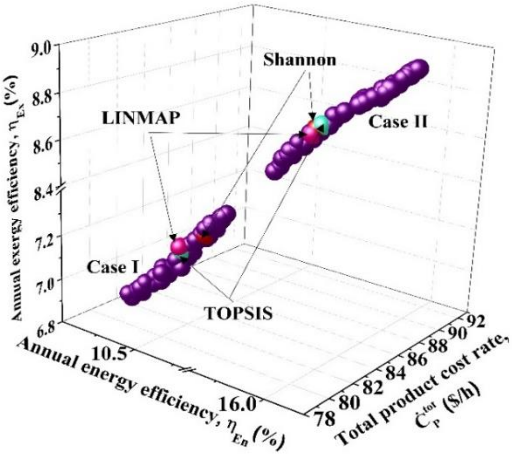

d) Total product EI rate and efficiencies

4. Conclusion:

A solar driven CCP based on CORC with three configurations of ERL is studied using thermodynamic, economic and EI analyses in the present work. The performances of the system are evaluated during a year and the impacts of design parameters are conducted on the annual performances of the system for various cases. Finally, the optimum operations of systems are found using NSGA-II and three decision makings. The major results are written here as follows:

- The highest improvement in product cost rate occurs in Case III within 2.448 $/s in relation to Case I.
- The amount of LNG produced in Case II gets 2 times in comparison with cases I and III leading to improvements in energy efficiency, exergy efficiency and economic performance of the system by about 43.2%, 8.23% and 1.1%, respectively.
- Case II leads to the minimum cost and EI per exergy unit of LNG within 0.03 $/GJ and 17 mPts/GJ, respectively and Case III gives the maximum total cost rate of 78.372 $/h.
- The increase of LNG mass flow rate extraction has the highest positive effect on the energy efficiency of Case I within 3%.
- The TUR-2 inlet pressure growth has the substantial influence on the exergy efficiency of Case II by about 4.42%.
- The total product cost rates of system are improved by about 1.78%, 1.94% and 1.96% respectively for Case I, Case II and Case III as the EJC-2 primary pressure increases.

  LINMAP decision making causes the maximum reduction in total product cost rates within 1.2% and 2.2%, respectively and improves the EI rates of cases I and II respectively up to 16 mPts/GJ and 7 mPts/GJ, respectively.

Tables 11. Results obtained from the exergy, exergoeconomic and exergoenvironmental analyses for Case I

Components	Exergy analysis		Exergoeconomic analysis							Exergoenvironmental analysis						
	$\dot{E}x_D$ (kW)	y_D (%)	c_P ($/GJ)	c_F ($/GJ)	$\dot{Z}$ ($/h)	$\dot{C}_D$ ($/h)	$\dot{Z}+\dot{C}_D$ ($/h)	r_c	f_c (%)	b_P (Pts/GJ)	b_F (Pts/GJ)	$\dot{Y}$ (Pts/h)	$\dot{B}_D$ (Pts/h)	$\dot{Y}_D+\dot{B}_D$ (Pts/h)	r_b	f_b (%)
LFC	8,783.0	74.27	4.679	0	51.23	0	51.23	∞	100	1.584	0	4.817	0	4.817	∞	100
TST	2,450.0	20.72	25.77	8.431	2.468	74.38	76.85	2.056	3.2	11.61	3.881	0.003	9.51	9.513	1.991	0.03
CON-2	1170.0	9.894	1.618	0.429	0.127	1.809	1.94	2.767	6.5	58.25	26.52	0.175	31.02	31.19	1.197	0.56
CON-1	319.7	2.703	2.303	0.429	0.024	0.494	0.518	4.361	4.6	137.2	26.52	0.022	8.478	8.5	4.172	0.26
LHE-1	268.1	2.268	19.70	14.24	0.434	13.75	14.18	0.384	3.1	71.75	52.20	0.109	13.99	14.09	0.375	0.77
HHE-2	150.0	1.268	68.70	25.80	0.504	13.91	14.41	1.666	3.5	31.69	11.61	0.132	1.741	1.873	1.730	7.06
EVP-1	104.4	0.883	53.02	11.65	0.044	4.38	4.42	3.549	1.0	277.1	63.04	0.016	6.397	6.413	3.520	0.25
EJC-1	94.4	0.031	92.66	36.2	0.000	12.31	12.31	3.371	00.0	153.1	143.7	0.000	4.561	4.561	3.371	00.00
TUR-2	81.2	0.687	30.18	19.70	5.713	5.76	11.47	0.532	49.8	90.97	71.75	0.020	5.825	5.845	0.268	0.35
TUR-1	47.5	0.402	37.94	27.33	4.957	4.676	9.63	0.388	51.5	63.04	52.99	0.020	2.517	2.537	0.189	0.80
EVP-2	32.7	0.277	3.886	1.451	4.363	0.171	4.53	1.679	96.2	61.16	52.24	2.90	1.710	4.610	0.171	62.93
HHE-1	30.5	0.258	31.97	25.77	0.755	2.831	3.59	0.241	21.1	15.20	11.61	0.222	0.354	0.576	0.309	38.56
CHE	30.0	0.254	11.65	11.19	0.588	1.21	1.79	0.042	32.7	61.27	59.47	0.161	1.784	1.945	0.031	8.29
P-3	9.7	0.082	177.4	37.94	0.158	1.328	1.486	3.677	10.6	270.4	63.04	0.001	0.613	0.614	3.290	0.09
PRC-1	7.3	0.061	36.64	11.14	0.118	0.291	0.409	2.289	28.8	218.4	81.32	0.021	0.590	0.611	1.686	3.37
EJC-2	3.685	0.799	158.2	86.99	0.000	1.154	1.15	0.065	00.0	211.1	143.7	0.000	0.529	0.529	0.065	00.00
REG	2.6	0.022	6.540	6.484	0.175	0.062	0.237	0.009	73.9	56.41	56.27	0.034	0.149	0.183	0.003	18.63
PRC-2	2.5	0.021	4.088	1.596	0.126	0.014	0.140	1.561	89.8	62.21	52.42	0.022	0.131	0.153	0.187	14.61
P-1	1.1	0.009	43.20	37.94	0.186	0.153	0.339	0.139	54.9	65.74	63.04	0.001	0.071	0.072	0.063	0.79
P-2	0.3	0.002	39.32	30.18	0.102	0.032	0.134	0.302	76.3	97.67	90.97	0.001	0.026	0.027	0.073	2.09
System	13,588.7	-	72.00	-	72.07	138.720	210.790	-	-	215.17	-	8.677	89.996	98.673	-	-

Tables 12. Results obtained from the exergy, exergoeconomic and exergoenvironmental analyses for Case II

Components	Exergy analysis		Exergoeconomic analysis							Exergoenvironmental analysis						
	$\dot{E}x_D$ (kW)	y_D (%)	c_P ($/GJ)	c_F ($/GJ)	$\dot{Z}$ ($/h)	$\dot{C}_D$ ($/h)	$\dot{Z}+\dot{C}_D$ ($/h)	r_c	f_c (%)	b_P (Pts/GJ)	b_F (Pts/GJ)	$\dot{Y}$ (Pts/h)	$\dot{B}_D$ (Pts/h)	$\dot{Y}_D+\dot{B}_D$ (Pts/h)	r_b	f_b (%)
LFC	8,894	62.77	4.858	0	51.23	0	51.23	-	100	0.457	0	4.817	0	4.817	-	100
TST	2,293	16.18	24.13	8.662	2.468	71.50	73.96	1.786	3.337	3.229	1.184	0.003	9.774	9.777	1.727	0.027
CON-2	1475	10.41	1.726	0.426	0.138	2.262	2.400	3.053	5.766	16.22	7.350	0.195	39.06	39.25	1.206	0.496
LHE-1	348.6	2.460	23.03	16.44	0.552	20.63	21.18	0.401	2.605	23.13	16.60	0.149	20.83	20.98	0.394	0.709
CON-1	318.7	2.249	2.279	0.426	0.024	0.489	0.512	4.352	4.650	37.93	33.34	0.022	8.435	8.456	4.160	0.256
EVP-1	222.2	1.568	63.55	14.57	0.092	11.65	11.74	3.363	0.783	86.24	19.85	0.036	15.88	15.91	3.345	0.227
EJC-1	143.8	1.015	169.1	49.57	0	25.66	25.66	2.412	0	113.7	33.34	0.000	17.25	17.25	2.412	0
HHE-2	130.8	0.923	56.69	24.13	0.505	11.37	11.87	1.349	4.258	7.763	3.229	0.133	1.521	1.654	1.404	8.037
EJC-2	100.8	0.711	65.07	34.48	0	12.51	12.51	0.887	0	23.01	12.19	0.000	4.424	4.424	0.887	0
TUR-2	95.75	0.676	36.26	23.03	5.357	7.938	13.29	0.574	40.29	31.08	23.13	0.020	7.974	7.994	0.344	0.256
EVP-2	49.82	0.352	3.356	1.584	3.374	0.284	3.658	1.119	92.23	17.22	14.88	0.000	2.669	2.669	0.158	44.81
HHE-1	30.63	0.216	30.07	24.13	0.727	2.661	3.388	0.246	21.46	4.224	3.229	0.133	0.356	0.489	0.308	37.30
TUR-1	22.97	0.162	36.55	26.31	3.340	2.176	5.516	0.389	60.55	17.73	15.33	0.020	1.268	1.289	0.156	1.586
REG	10.97	0.077	9.634	9.536	0.107	0.377	0.484	0.010	22.13	19.38	19.23	0.018	0.760	0.778	0.008	2.336
PRC-1	10.82	0.076	36.41	13.02	0.063	0.507	0.570	1.796	32.39	55.82	24.48	0.052	0.954	1.006	1.28	5.168
P-3	10.64	0.075	171.3	36.55	0.163	1.400	1.563	3.687	10.45	76.30	17.73	0.001	0.679	0.680	3.305	0.083
CHE	7.417	0.052	14.57	14.31	0.832	0.382	1.215	0.018	68.53	19.85	19.69	0.252	0.526	0.777	0.008	32.38
PRC-2	2.217	0.016	5.391	1.750	0.438	0.014	0.452	2.080	96.91	16.8	14.95	0.111	0.119	0.230	0.124	48.12
P-1	1.122	0.008	41.72	36.55	0.186	0.148	0.334	0.142	55.78	18.84	17.73	0.001	0.072	0.072	0.063	0.782
P-2	0.359	0.003	45.02	36.26	0.111	0.047	0.157	0.242	70.26	33.34	31.08	0.001	0.040	0.041	0.073	1.386
System	14,169.6	-	76.166	-	69.71	172	241.7	-	-	66.03	328.5	5.96	132.6	138.5	-	-

Tables 13. Results obtained from the exergy, exergoeconomic and exergoenvironmental analyses for Case III

Components	Exergy analysis		Exergoeconomic analysis							Exergoenvironmental analysis						
	$\dot{E}x_D$ (kW)	y_D (%)	c_P ($/GJ)	c_F ($/GJ)	$\dot{Z}$ ($/h)	$\dot{C}_D$ ($/h)	$\dot{Z}+\dot{C}_D$ ($/h)	r_c	f_c (%)	b_P (Pts/GJ)	b_F (Pts/GJ)	$\dot{Y}$ (Pts/h)	$\dot{B}_D$ (Pts/h)	$\dot{Y}_D+\dot{B}_D$ (Pts/h)	r_b	f_b (%)
LFC	8783	74.28	4.68	0	51.23	0.000	51.23	∞	100.0	0.440	0	4.817	0.000	4.817	∞	100
TST	2450	20.72	26.1	8.53	2.468	75.24	77.71	2.056	3.177	3.491	1.167	0.003	10.30	10.30	1.991	0.026
CON-2	1206	10.20	1.87	0.435	0.117	1.891	2.008	3.299	5.848	16.36	7.373	0.159	32.01	32.17	1.219	0.493
CON-1	317	2.68	2.32	0.435	0.024	0.498	0.521	4.329	4.590	37.90	7.373	0.022	8.420	8.442	4.141	0.257
LHE-1	259	2.19	26.5	19.41	0.477	18.12	18.59	0.367	2.566	26.19	19.25	0.123	17.97	18.09	0.360	0.682
EJC-2	177	1.50	282	33.98	0.000	21.64	21.64	7.301	0.000	125.6	15.13	0.000	9.634	9.634	7.301	0.000
HHE-2	150	1.27	69.5	26.06	0.504	14.07	14.58	1.665	3.457	9.499	3.491	0.132	1.885	2.018	1.721	6.559
EJC-1	135	1.14	2568	64.80	0.000	31.47	31.47	38.63	0.000	1722	43.44	0.000	21.10	21.10	38.63	0.000
EVP-1	103	0.87	82.0	17.91	0.043	6.631	6.674	3.579	0.648	104.1	22.81	0.015	8.446	8.461	3.562	0.181
TUR-2	55.9	0.47	38.1	57.69	4.831	11.61	16.44	0.339	29.39	32.22	56.93	0.020	11.46	11.48	0.434	0.178
EVP-2	38.7	0.33	3.60	1.716	3.087	0.239	3.326	1.100	92.81	17.30	15.00	1.959	2.090	4.049	0.153	48.39
CHE	37.1	0.31	17.9	17.17	0.572	2.293	2.865	0.043	19.97	22.81	22.00	0.156	2.939	3.095	0.037	5.035
TUR-1	34.1	0.29	40.8	29.91	4.162	3.672	7.834	0.364	53.13	20.01	17.07	0.020	2.095	2.115	0.172	0.966
HHE-1	30.5	0.26	32.3	26.06	0.755	2.864	3.619	0.240	20.87	4.539	3.491	0.222	0.384	0.606	0.300	36.69
P-3	9.73	0.08	190	40.79	0.158	1.428	1.586	3.649	9.938	85.81	20.01	0.001	0.701	0.701	3.289	0.080
REG	7.57	0.06	10.9	10.84	0.068	0.295	0.364	0.008	18.74	20.37	20.23	0.010	0.552	0.562	0.007	1.812
PRC-1	7.26	0.06	48.3	15.58	0.118	0.407	0.525	2.101	22.46	71.30	26.63	0.021	0.696	0.716	1.677	2.871
PRC-2	2.70	0.02	4.40	1.893	0.130	0.018	0.149	1.322	87.62	17.94	15.07	0.023	0.146	0.170	0.190	13.74
P-1	1.12	0.01	46.2	40.79	0.186	0.165	0.351	0.133	53.06	21.27	20.01	0.001	0.081	0.081	0.063	0.693
P-2	0.29	0.001	47.8	38.13	0.102	0.040	0.141	0.255	71.76	34.57	32.22	0.001	0.034	0.034	0.073	1.644
System	13805	-	3543	452.1	69.03	192.6	261.6	-	-	2393.7	368.7	7.705	130.9	138.636	-	-

Appendix A. The cost functions of main components of the system components are as follows:

Table A1. Equipment cost functions

Component	Cost function	Reference
TURs	$Z_{TUR} = 4750\left(\dot{W}_{TUR}\right)^{0.75} + 60\left(\dot{W}_{TUR}\right)^{0.95}$	[47]
TST	$Z_{TST} = 0.4\left(1380 \times \bar{V}_{TST}\right)$	[47]
Ps	$Z_P = 3500\left(\dot{W}_P\right)^{0.41}$	[47]
CONs	$Z_{CON} = 150\left(A_{CON}\right)^{0.8}$	[47]
HEx	$Z_{HE} = 130\left(A_{HE}/0.093\right)^{0.78}$	[47]
EVPs	$Z_{EVA} = 276\left(A_{EVA}\right)^{0.88}$	[47]
LFC	$Z_{LFC} = 200 \times A_{ap}$	[48]

Nomenclature:

A area, m^2
$\dot{B}$ environmental impact rate associated with an exergy stream, Pt/s
b specific environmental impact per unit of exergy, Pts/J
C concentration ratio
$\dot{C}$ cost rate of exergy stream, \$/s
c cost per unit of exergy, \$/J
Cp specific heat of fluid, kJ/kg.K
D diameter, m
$\dot{E}x$ total exergy rate, kW
ex specific exergy, kJ/kg
f_b exergoenvironmental factor
f_c exergoeconomic factor
G_b beam radiation falling on the horizontal surface, W/m^2
h specific enthalpy, kJ/kg
IR interest rate, %
$\dot{m}$ mass of fluid flow rate, kg/s
N system life, year
P pressure, kPa
$\dot{Q}$ heat transfer rate, kW
r shading factor
r_b relative environmental impact difference
r_c relative cost difference
s specific entropy, kJ/kg .K
S absorbed solar heat, W/m^2
t time, s
T temperature, K
U overall heat transfer coefficient, $W/m^2.K$
V velocity, m/s
w mirror width, m
$\dot{W}$ power rate, W
x quality

The capital investment cost functions
$\dot{Z}$ cost rate associated with investment expenditures, \$/s

Abbreviation

CHE cascade heat exchanger
CON condenser
CORC cascade organic Rankine cycle
CRF capital recovery factor
EI environmental impact
EJC ejector
ERL ejector refrigeration loop
EVP evaporator
HHE high temperature heat exchanger
LFC linear Fresnel solar collector
LHE low temperature heat exchanger
LNG liquefied natural gas
NG natural gas
ORC organic Rankine cycle
P pump
PRC precooler
REG regenerator
TST thermal storage tank
TUR turbine
TV throttling valve

Subscript

0 dead state
air air
ap aperture
D destruction
d diffuser
En energy
Ex exergy
F fuel
g glass cover
i inner
in input
inlet inlet
is isentropic
k *k*th component
L loss
load load
mn motive nozzle
ms mixing section
net net
oil Therminol-PV1
outlet outlet
P product
q heat transfer
r receiver
sn suction nozzle
u useful
w power

Superscript

ch chemical
M mechanical

$\dot{Y}$	component-related environmental impact rate, Pt/s
Z	cost associated with investment expenditures, $

Greek letter

α	absorptivity
γ	refelectivity
ε	emissivity of the surface
ρ	density, kg/m^3
σ	Stefan–Boltzman constant, W/m^2.K^4
τ	transitivity

ph	physical
T	thermal
tot	total

η	efficiency, %
θ	tilt angle, º
φ	maintenance factor
μ	entrainment ratio

References:

1. Al-Sulaiman, F.A., I. Dincer, and F. Hamdullahpur, *Exergy modeling of a new solar driven trigeneration system.* Solar Energy, 2011. **85**(9): p. 2228-2243.
2. Wang, E., et al., *Performance analysis of a novel system combining a dual loop organic Rankine cycle (ORC) with a gasoline engine.* Energy, 2012. **43**(1): p. 385-395.
3. Choi, B.C. and Y.M. Kim, *Thermodynamic analysis of a dual loop heat recovery system with trilateral cycle applied to exhaust gases of internal combustion engine for propulsion of the 6800 TEU container ship.* Energy, 2013. **58**: p. 404-416.
4. Shu, G., et al., *Performance comparison and working fluid analysis of subcritical and transcritical dual-loop organic Rankine cycle (DORC) used in engine waste heat recovery.* Energy conversion and management, 2013. **74**: p. 35-43.
5. Zhang, H., E. Wang, and B. Fan, *A performance analysis of a novel system of a dual loop bottoming organic Rankine cycle (ORC) with a light-duty diesel engine.* Applied energy, 2013. **102**: p. 1504-1513.
6. Wang, E., et al., *Parametric analysis of a dual-loop ORC system for waste heat recovery of a diesel engine.* Applied Thermal Engineering, 2014. **67**(1): p. 168-178.
7. Yang, F., et al., *Performance analysis of waste heat recovery with a dual loop organic Rankine cycle (ORC) system for diesel engine under various operating conditions.* Energy Conversion and Management, 2014. **80**: p. 243-255.
8. Pouraghaie, M., et al., *Thermodynamic performance optimization of a combined power/cooling cycle.* Energy Conversion and Management, 2010. **51**(1): p. 204-211.
9. Jiang, L., et al., *Investigation on cascading cogeneration system of ORC (Organic Rankine Cycle) and CaCl2/BaCl2 two-stage adsorption freezer.* Energy, 2014. **71**: p. 377-387.
10. Wang, L., A.P. Roskilly, and R. Wang, *Solar powered cascading cogeneration cycle with ORC and adsorption technology for electricity and refrigeration.* Heat Transfer Engineering, 2014. **35**(11-12): p. 1028-1034.
11. Al-Mousawi, F.N., R. Al-Dadah, and S. Mahmoud, *Integrated adsorption-ORC system: Comparative study of four scenarios to generate cooling and power simultaneously.* Applied Thermal Engineering, 2017. **114**: p. 1038-1052
12. Sarkar, J., *Ejector enhanced vapor compression refrigeration and heat pump systems—A review.* Renewable and Sustainable Energy Reviews, 2012. **16**(9): p. 6647-6659.
13. Kornhauser, A.A., *The use of an ejector as a refrigerant expander.* 1990.
14. Harrell, G.S. and A.A. Kornhauser, *Performance tests of a two phase ejector*. 1995, American Society of Mechanical Engineers, New York, NY (United States).
15. Disawas, S. and S. Wongwises, *Experimental investigation on the performance of the refrigeration cycle using a two-phase ejector as an expansion device.* International Journal of Refrigeration, 2004. **27**(6): p. 587-594.
16. Wongwises, S. and S. Disawas, *Performance of the two-phase ejector expansion refrigeration cycle.* International journal of heat and mass transfer, 2005. **48**(19): p. 4282-4286.
17. Wang, J., Y. Dai, and Z. Sun, *A theoretical study on a novel combined power and ejector refrigeration cycle.* International Journal of Refrigeration, 2009. **32**(6): p. 1186-1194.
18. Habibzadeh, A., M. Rashidi, and N. Galanis, *Analysis of a combined power and ejector-refrigeration cycle using low temperature heat.* Energy Conversion and Management, 2013. **65**: p. 381-391.
19. Zheng, B. and Y. Weng, *A combined power and ejector refrigeration cycle for low temperature heat sources.* Solar Energy, 2010. **84**(5): p. 784-791.
20. Ahmadzadeh, A., M.R. Salimpour, and A. Sedaghat, *Thermal and exergoeconomic analysis of a novel solar driven combined power and ejector refrigeration (CPER) system.* International Journal of Refrigeration, 2017. **83**: p. 143-156.
21. Rostamzadeh, H., et al., *Energy and Exergy Analysis of Novel Combined Cooling and Power (CCP) Cycles.* Applied Thermal Engineering, 2017
22. Rostamzadeh, H., et al., *Exergoeconomic optimisation of basic and regenerative triple-evaporator combined power and refrigeration cycles.* International Journal of Exergy, 2018. **26**(1-2): p. 186-225.

23. Ebadollahi, M., et al., *Exergoeconomic analysis and optimization of innovative cascade bi-evaporator electricity/cooling cycles with two adjustable cooling temperatures.* Applied Thermal Engineering, 2019. **152**: p. 890-906.
24. Boyaghchi, F.A. and A. Sohbatloo, *Assessment and optimization of a novel solar driven natural gas liquefaction based on cascade ORC integrated with linear Fresnel collectors.* Energy Conversion and Management, 2018. **162**: p. 77-89.
25. El Gharbi, N., et al., *A comparative study between parabolic trough collector and linear Fresnel reflector technologies.* Energy Procedia, 2011. **6**: p. 565-572.
26. Goswami, D.Y. and F. Kreith, *Handbook of energy efficiency and renewable energy*. 2007: Crc Press.
27. Kalogirou, S.A., *Solar energy engineering: processes and systems*. 2013: Academic Press.
28. Häberle, A., et al. *The Solarmundo line focussing Fresnel collector. Optical and thermal performance and cost calculations*. in *Proceedings of the International Symposium on Concentrated Solar Power and Chemical Energy Technologies, SolarPACES, Zürich, Sep*. 2002.
29. Hu, E.J., et al. *Solar power boosting of fossil fuelled power plants*. in *Proceedings of the International Solar Energy Congress*. 2003.
30. Abbas, R., et al., *Solar radiation concentration features in Linear Fresnel Reflector arrays.* Energy Conversion and Management, 2012. **54**(1): p. 133-144.
31. Calm, J.M. and G.C. Hourahan, *Refrigerant data summary.* Engineered Systems, 2001. **18**(11): p. 74-88.
32. Li, H., et al., *Performance characteristics of R1234yf ejector-expansion refrigeration cycle.* Applied Energy, 2014. **121**: p. 96-103.
33. Sumeru, K., H. Nasution, and F. Ani, *A review on two-phase ejector as an expansion device in vapor compression refrigeration cycle.* Renewable and Sustainable Energy Reviews, 2012. **16**(7): p. 4927-4937.
34. Reddy, V.S., S. Kaushik, and S. Tyagi, *Exergetic analysis of solar concentrator aided natural gas fired combined cycle power plant.* Renewable Energy, 2012. **39**(1): p. 114-125.
35. Wang, M., et al., *Multi-objective optimization of a combined cooling, heating and power system driven by solar energy*. Energy Conversion and Management, 2015. **89**: p. 289-297.
36. Bejan, A. and G. Tsatsaronis, *Thermal design and optimization*. 1996: John Wiley & Sons.
37. Lazzaretto, A. and G. Tsatsaronis, *SPECO: a systematic and general methodology for calculating efficiencies and costs in thermal systems.* Energy, 2006. **31**(8-9): p. 1257-1289.
38. Ameri, M., P. Ahmadi, and A. Hamidi, *Energy, exergy and exergoeconomic analysis of a steam power plant: A case study.* International Journal of Energy Research, 2009. **33**(5): p. 499-512.
39. Boyaghchi, F.A. and P. Heidarnejad, *Thermodynamic analysis and optimisation of a solar combined cooling, heating and power system for a domestic application.* International journal of exergy, 2015. **16**(2): p. 139-168.
40. Meyer, L., et al., *Exergoenvironmental analysis for evaluation of the environmental impact of energy conversion systems.* Energy, 2009. **34**(1): p. 75-89.
41. Deb, K., et al., *A fast and elitist multiobjective genetic algorithm: NSGA-II.* IEEE transactions on evolutionary computation, 2002. **6**(2): p. 182-197.
42. Ahmadi, M.H., et al., *Application of the multi-objective optimization method for designing a powered Stirling heat engine: design with maximized power, thermal efficiency and minimized pressure loss.* Renewable Energy, 2013. **60**: p. 313-322.
43. Sayyaadi, H. and R. Mehrabipour, *Efficiency enhancement of a gas turbine cycle using an optimized tubular recuperative heat exchanger.* Energy, 2012. **38**(1): p. 362-375.
44. Guisado, J.L., F. Jiménez-Morales, and J.M. Guerra, *Application of shannon's entropy to classify emergent behaviors in a simulation of laser dynamics.* Mathematical and computer modelling, 2005. **42**(7-8): p. 847-854.
45. Li, Y., S. Liao, and G. Liu, *Thermo-economic multi-objective optimization for a solar-dish Brayton system using NSGA-II and decision making.* International Journal of Electrical Power & Energy Systems, 2015. **64**: p. 167-175.
46. Zheng, B. and Y.W. Weng, *A combined power and ejector refrigeration cycle for low temperature heat sources.* Solar Energy, 2010. **84**(5): p. 784-791.
47. Boyaghchi, F.A., M. Chavoshi, and V. Sabeti, *Optimization of a novel combined cooling, heating and power cycle driven by geothermal and solar energies using the water/CuO (copper oxide) nanofluid.* Energy, 2015. **91**: p. 685-699.
48. Morin, G., et al., *Comparison of linear Fresnel and parabolic trough collector power plants.* Solar Energy, 2012. **86**(1): p. 1-12.